An Interpretation of Spacecraft and Ground Based Observations of Multiple Omega Band Events

J.M. Weygand[1,2], M.G. Kivelson[1, 2], H. U. Frey[3], J.V. Rodriguez[4,5], V. Angelopoulos[1, 2], R. Redmon[5], J. Barker-Ream[1,2,] A. Grocott[6], O. Amm[7]

[1] Institute of Geophysics and Planetary Physics, University of California Los Angeles, Los Angeles, CA , USA

[2] Department of Earth, Planetary, and Space Sciences, University of California Los Angeles, Los Angeles, CA, USA

[3] Space Sciences Laboratory, University of California, Berkeley, CA, USA

[4] Cooperative Institute for Research in Environmental Sciences, University of Colorado Boulder, 216 UCB, Boulder, CO 80309 USA

[5] National Oceanic and Atmospheric Administration/National Geophysical Data Center 325 Broadway E/GC2 Boulder, CO 80305, USA

[6] Department of Physics and Astronomy, University of Leicester, UK

[7] Finnish Meteorological Institute, Finland

Corresponding Author: J.M. Weygand (jweygand@igpp.ucla.edu). Phone: 310 825 3547

Short title: March 9, 2008 Omega Bands

Submitted to the Journal of Atmospheric and Solar-Terrestrial Physics

UCLA Institute of Geophysics and Planetary Physics

Department of Earth, Planetary, and Space Science

August 1, 2015

Abstract

The source of the auroral phenomenon known as omega bands is not yet known. We examine in detail five different intervals when omega bands were observed on March 9th, 2008 between 0400 UT and 1100 UT over central Canada using both ground and space-based instrumentation. The THEMIS all sky imagers show the development of some of the omega bands from north-south streamers. Spherical elementary currents derived from ground magnetometer data indicate that the omega bands lie near the interface between the region 1and region 2 currents in the post midnight sector. THEMIS spacecraft data from the pre-midnight sector display multiple high speed flows and dipolarization features associated with high levels of geomagnetic activity, whereas four GOES geosynchronous spacecraft show multiple injections and dipolarization features. Magnetic field line tracing suggests that the magnetospheric location of the omega bands is at or just beyond geosynchronous orbit. We discuss in detail two potential source mechanisms for the omega bands: plasma sheet velocity shears and high speed flows in the magnetotail and relate the available data to those mechanisms. Our data and a magnetohydrodynamic (MHD) simulation support high speed flows in the magnetotail as the most likely generation mechanism, although the distribution of the magnetotail spacecraft does not provide unambiguous support for our interpretation of the source mechanism.

1. Introduction

Akasofu and Kimball [1964] were the first to describe the auroral wave-like structures called "omega bands", which appear within the morning sector auroral oval with shapes resembling the Greek letter Ω, and are typically associated with the recovery phase of magnetic substorms [*Vanhamäki et al.,* 2009]. To date, the generation mechanism for this auroral phenomenon has not yet been established and the available information comes mainly from ground observations. Omega bands typically consist of several equally spaced structures that propagate from west to east with a speed of 400 to 2000 m/s [*Yamamoto et al.*, 1993*; Opgenoorth et al.*, 1983; *Mravlag et al.,* 1991] consistent with the average $\vec{E} \times \vec{B}$ plasma drift velocity [*André and Baumjohann,* 1982]. Auroral observations of omega bands have been recorded in both hemispheres on the same day, which suggests they may be conjugate in both hemispheres, but the observations were not at the exact same time [*Mravlag et al.*, 1991].

Saito [1978] was the first to propose a connection between the occurrence of omega bands and magnetic Ps6 pulsations, which have periods of 5 to 40 min and amplitude from 10 to 1200 nT [*Saito*, 1977]. This connection was confirmed by *André and Baumjohann* [1982]. Ps6 pulsations, which are pulsations associated with substorms, are believed to be the magnetic signature of the ionospheric current system associated with omega bands drifting eastward over a ground magnetometer station. Ground magnetometer observations do not display special characteristics in the *Bx* component that points toward the geographic north pole in the center of a single omega, but the *By* component that points toward geographic east displays a sharp, spike like increase associated with the western edge. The *Bz* component that points into the Earth has a sawtooth form, with a minimum eastward of the center of the omega band and a sharp increase on the western side. [See Figure 3 of *Jorgensen et al.*, 1999].

The fluctuations observed in all three components of the magnetic field show that a three-dimensional ionospheric current system is present. A great deal of work has been done on the three-dimensional current system of omega bands [*Kawasaki and Rostoker*, 1979; *Gustafsson et al.*, 1981; *André and Baumjohann*, 1982; *Opgenoorth et al.*, 1983; *Lühr and Schlegel*, 1994, *Amm*, 1996]. In general, the brightest edges of the omega bands lie near the interface between the region 1 and region 2 current system in the morning sector.

A number of studies have used magnetic field models to identify the magnetospheric equatorial location of the observed omega bands mapped along field lines [*Pulkkinen et al*. 1991; *Tagirov*, 1993; and *Wild et al*. 2011]. *Pulkkinen et al*. [1991] determined that the omega bands observed on March 25, 1986 mapped to 6 to 13 R_E with Tsyganenko's 1989 (T89) magnetic field model [*Tsyganenko*, 1989] and *Tagirov* [1993] found that the omega bands observed on April 9-10, 1986 mapped to 5 to 6 R_E, also using the T89 model. The omega bands observed over Iceland with the Tjörnes all sky imager on September 28, 2009 [*Wild et al.*, 2011] were found to be conjugate with the Cluster spacecraft at about 8 Re down tail on the basis of field line tracing with the Tsyganenko 2001 model [*Tsyganenko*, 2002a; 2002b].

Ground based observations of omega bands are relatively common; however, spacecraft measurements of the magnetospheric signature of omega bands are less common. The bulk of spacecraft observations are from auroral imagers such as Viking, IMAGE, and Polar [*Henderson*, 2009; 2012; *Henderson et al.*, 1998; 2002; *Opgenoorth et al.*, 1994; *Amm et al.*, 2005]. As far as we are aware, only the *Wild et al.* [2011] study provides spacecraft observations in the magnetotail on or near magnetic field lines conjugate to auroral omega bands. The *Wild et al.* [2011] study did not show a one-to-one correlation between the auroral structures and the *in situ* plasma or magnetic observations, but did show enhanced Alfvénic Poynting flux and transient bursts of electron differential energy flux with dispersed energy signatures throughout the event when satellite foot points were located in the vicinity of the omega bands.

We do not yet understand what causes omega bands to develop. It is most likely that the paucity of concurrent magnetospheric measurements has limited our ability to understand why they occur. However, a number of mechanisms, which are reviewed in *Amm et al*. [2005], have been proposed. The most widely accepted generation mechanisms are that omega bands form as a direct consequence of auroral streamer activity [*Roux et al*., 1991; *Henderson*, 2009; 2012], where auroral streamers are the ionospheric projection of earthward flow burst in the plasma sheet [*Nishimura et al.*, 2011], or that they arise through the structuring of magnetic vorticity and field-aligned currents in the ionosphere by the Kelvin Helmholtz instability driven by flow shears at the inner edge of the plasma sheet [*Rostoker and Samson* 1984, *Janhunen and Huuskonen*, 1993]. The auroral streamer/high speed flow mechanism predicts that spacecraft in the tail should observe high speed earthward flows with field aligned currents at the flow shears, magnetic field dipolarizations associated with the high speed flows, and particle enhancements near geosynchronous orbit. The flow shear mechanism predicts flow shears within the tail at about 6-13 Re, oscillation in the radial component of the magnetic field near the shear, and the region 1 currents should exceed the region 2 currents prior to the flow shear but the currents are approximately equal during the omega bands.

The goal of our study is to use ground and space-based observations to examine in detail five periods of omega bands that appeared on March 9, 2008 and to suggest a possible generation mechanism. In the next section we discuss the ground and space-based instrumentation used in our study. In section 3 we discuss in detail the available observations and in the last two sections we interpret the observations, then summarize and conclude.

2. Spacecraft and Instrumentation

The data for this study come from four sources: the Time History of Events and Macroscale Interactions During Substorms (THEMIS) all-sky image (ASI) array, the THEMIS spacecraft, four Geostationary Operational Environmental Satellites (GOES), and seven ground magnetometer arrays.

THEMIS ASIs are used to identify the omega bands. White light ASIs are obtained from an array of Ground-Based Observatories (GBOs) spread over Alaska and Canada. **Figure 1** shows the location of the ASIs (orange diamonds) as well as the ground magnetometers (black dots), the average location of the GOES spacecraft foot points (yellow squares) determined from magnetic field line mapping with T89, T96, and T01 over 04 UT to 11 UT, and the THEMIS C (green), D (mauve), and E (blue) spacecraft foot points for the events that we investigate. The THEMIS spacecraft foot points start at 04 UT at the lowest latitude and end in Alaska at 11 UT. Each all sky imager has a cadence of 3 s and a spatial resolution of 1 km at zenith. The spatial resolution decreases to about 2.5 km at an elevation angle of 45° and dramatically diminishes to about 15 km at an elevation angle of 15°. More details on the imagers and their geographic positions can be found in *Donovan et al.* [2006] and *Mende et al.* [2008]. The ASIs are an essential part of the THEMIS spacecraft mission. These imagers, along with the ground magnetometers, and spacecraft instruments provide a global picture of magnetosphere-ionosphere coupling.

The main objective of the THEMIS spacecraft mission is to identify the chain of events that leads to substorms [*Angelopoulos*, 2008] but the combination of ground-based instrumentation with multiple equatorial spacecraft is of great value for investigation of other magnetospheric phenomena including the study of omega bands. The THEMIS mission consists of 5 identical spacecraft, initially placed in elliptical orbits with different apogees that align every 4 days. In 2007-2009, three of the spacecraft had apogees around 10 R_E, one had an apogee at about 20 R_E and one had an apogee near 30 R_E. Each spacecraft has 5 instruments and we will examine data from the ElectroStatic Analyzer (ESA) and the FluxGate Magnetometer (FGM). ESA [*McFadden et al., 2008*] provides fundamental plasma parameters such as density, velocity vectors, the pressure tensor, heat flux, and the ion and electron distribution functions. These data are used to characterize the plasma flows within the magnetotail. The uncertainties associated with the plasma sheet flow used in this study are less than 10%.

Each THEMIS spacecraft carries a boom-mounted triaxial fluxgate magnetometer (FGM) [*Auster et al.*, 2008]. Magnetic field vectors routinely are available at 64 Hz resolution (nominal mode). The absolute uncertainty in the data after calibration is at most 0.1 nT, an estimate determined by examining the drift in the offset after calibration [*H. Leinweber*, personal communication, 2010]. However, the digital resolution, short-term stability, and noise level of the magnetometer are on the order of 0.01 nT [*Auster et al.*, 2008].

During the omega band event examined in this study we are fortunate to have data from 4 different GOES spacecraft (GOES 10-13) positioned over North America. Figure 1 shows the locations of the foot points (yellow squares). From GOES 10-12 we use the fluxgate magnetometer data at 0.5 s resolution [*Singer et al.*, 1996] and the Energetic Particles Sensor data from the Solar Environment Monitor (SEM) at 5 min resolution [*Onsager et al.*, 1996]. From the GOES 13 spacecraft we also use the fluxgate magnetometer data at 0.5 s resolution and particle data from the Magnetospheric Electron Detector (MAGED) with temporal resolutions ranging from 2 s to 6 s depending on the channel within the 30-600 keV energy range [*Hanser*, 2011; *Jaynes et al.*, 2013].

We have obtained data from seven different ground magnetometer arrays: CANMOS (CANadian Magnetic Observatory System), CARISMA (Canadian Array for Real time Investigations of Magnetic Activity) [*Mann et al.*, 2008], GIMA (Geophysical Institute Magnetometer Array), Technical University of Denmark (DTU) Magnetometer Ground Stations in Greenland [http://www.space.dtu.dk/MagneticGroundStations], MACCS (Magnetometer Array for Cusp and Cleft Studies) [*Engebretson et al.*, 1995], the STEP (Solar-Terrestrial Energy Program) magnetometer array [http://step-p.dyndns.org/~khay/], and THEMIS GMAG [*Russell et al*., 2008]. The locations of the magnetometers with good data for the omega band periods are shown as black dots in Figure 1. Many of the ground magnetometer arrays share some stations; all of the data from GIMA, MACCS, and the Greenland stations used in this study can be obtained from the THEMIS GMAG online data archive, whereas the rest were obtained from the original provider. In total we have data from nearly 80 stations.

We use the ground magnetometer data with 10 s time resolution to calculate the equivalent ionospheric currents and vertical (close to field-aligned) currents using the spherical elementary current system (SECS) method [*Amm and Viljannen*, 1999]. The spatial resolution of the equivalent ionospheric currents is about 2.9° in geographic latitude and 6.9° in geographic longitude, and the spatial resolution of the vertical currents is about 1.5° in geographic latitude and 3.5° in geographic longitude. This difference in resolution results from use of the SECS method for evaluating the currents (See *Amm and Viljannen* [1999] for more details). The SECS method assumes that the magnetic field fluctuations recorded by the ground magnetometers come only from ionospheric currents located 100 km above the surface. More details on the method used to calculate the spherical elementary currents (SECs) can be found in *Amm and Viljanen* [1999] and the description of the SECS applied over over North America and Greenland and *Weygand et al.* [2011; 2012].

3. Data

The first of five groups of omega bands is observed by the THEMIS GBOs over central Canada at about 0439 UT on March 9th, 2008 just after magnetic local midnight. Our operational definition of omega bands is auroral shapes that propagate towards dawn at the equatorward portion of the oval resembling the Greek letter Ω that have an amplitude of 0.4° or greater with a base of about the same width as the amplitude or less. **Figure 2** shows 8 mosaics from the ASIs at times given in the lower left corners of the images. The eleven ASIs that provide the mosaic images shown in each panel of **Figure 2** provide the best views of the omega bands. The images to the west show either clouds or are located too far north to capture the omega bands. Table 1 summarizes the time periods and the specific imagers that display omega bands during the five different time intervals. In **Panel A** of Figure 2, we have labeled some the ASIs to which we will refer. This panel shows a number of streamers (i.e., north-south structures in the aurora [*Henderson*, 1994; *Elphinstone et al.,* 1995; *Sergeev et al.,* [1999]) that propagate from the northern edge of the auroral oval to the southern edge of the auroral oval. Auroral streamers are the ionospheric projection of upward field-aligned currents forming on the western edge of earthward flow burst in the plasma sheet [*Nishimura et al.,* 2011]. The bright streamer at about 270° geographic longitude (GLon) starting at the southern edge of the RANK ASI (62.8° geographic latitude (GLat), 267.9° Glon) evolves into the omega band seen in **Panel B** in the KAPU ASI (49.4° GLat, 277.7° GLon). Several minutes later another omega band forms and these omega bands propagate to the east. By 0443 UT they have decayed or propagated out of the field of view of all of the ASIs. **Panel C** shows a single omega band in the GBAY ASI (53.3° GLat, 299.5° GLon). Unfortunately, we did not see this omega band form before it propagated into the field of view from the west. It is unclear if this omega band is related to those observed in **Panel B**. **Panel D** shows another streamer, which begins at about 0606 UT, extending from the GILL ASI (56.4° GLat, 265.3° GLon) down to TPAS (54.0° GLat, 259.0° GLon). The northern end of the streamer moves equatorward and eventually evolves into two large omega bands that drift eastward and can be seen in **Panel E**. Two smaller omega-band-like features form to the east over KAPU at about 0622 UT. All the omega bands drift eastward, shrink, and then appear to break apart at about 0631:30 UT. Shortly after the disappearance of these small omega bands, another bright north-south arc appears over FSMI and breaks up by 0647 UT leaving behind a great deal of auroral activity over ATHA, FSIM, FSMI, and YKNF, which spreads eastward to KAPU by 0706 UT. At 0644 UT, during the auroral oval activity, a fourth set of large omega bands forms just where (over GILL) the omega bands formed in the third interval. **Panel F** shows several of the omega bands from the fourth interval. These omega bands do not appear to be associated with any streamers and seem to form from the remains of the previously identified omega bands. The fourth group of omega bands either propagates to the east out of the field of view of the KAPU all sky imager or break apart by 0658 UT. After this set of omega bands disappears, the poleward edge of the auroral oval brightens twice. The first brightening occurs at about 0722 UT at the northern edge of the auroral oval over INUV, FSIM, YKNF, and FSMI. The activity begins to fade at about 0758 UT. The second poleward brightening occurs at approximately 0817 UT over INUV and spreads to FSIM, YKNF, and FSMI by 0819 UT and the breakup begins at 0824 UT.

The fifth episode of omega bands starts at 0826:30 UT over ATHA (54.7° GLat, 246.7° GLon) at about local midnight. The omega bands drift eastward for about 2 to 3 hours in local time. **Panels G and H** show two mosaics from the last interval of omega bands. In total 16 omega bands are observed drifting from the ATHA imager eastward and shrinking to nothing before reaching the SNKQ ASI (56.5° geographic north, 280.8° geographic east). At about 0854 UT several very large omega bands appear. One omega band displays ripples on its northeastern edge. These large omega bands begin to fade by 0930 UT, but smaller ones continue until 1003 UT. Between 0950 UT and 1011 UT there is a brief break in the train of omega bands, then more omega bands propagate into the field of view from the west. By 1054 UT all the omega bands have decayed away.

A movie of consisting of all the omega band intervals and a time line of all the events that occur during the period considered in this study has been submitted as supplementary data. These supplementary materials are meant to provide better context for the observations.

The omega bands develop during relatively active magnetospheric conditions. The omega bands occur about 0430 UT, 3 hours after the magnetosphere encounters a corotating interaction region at 0130 UT. At about the same time as the arrival of the corotating interaction region the AE and AL indices begin to increase in magnitude, which ends at about 1300 UT, March 9th, 2008 [*Jian et al.*, 2011; *Paroomian et al.*, 2014]. The first interval of omega bands starts during a period of very active geomagnetic conditions when the AE and AL indices reach about 1000 and -800 nT, respectively. **Figure 3** displays geomagnetic indices, IMF, and solar wind plasma properties from 0400 UT to 1100 UT covering the intervals during which the omega bands form. The AE and AL indices are given in the top panel. The gray patches, which mark the 5 different intervals of omega bands, show that they occur at times of moderate or exceptionally high geomagnetic activity. The AE index is greater than 200 nT for all the omega band intervals. At about 0513 UT and 0657 UT, there are sharp drops in the AL index. The first drop at 0513 UT is associated with a sharp rotation in all three IMF components. However, no clear substorm signatures are evident in the THEMIS ASIs or ground magnetometer data at this time. The second sharp drop in AL at 0657 UT is associated with strong tailward bursty bulk flows at THC, THD, and THE; and a dispersionless particle injection is observed at GOES 13, consistent with substorm activity.

The Sym-H (gray curve) and Asym-H (gold curve) indices shown in the second panel of **Figure 3** reveal that these omega band events take place during a magnetic storm, which reached a minimum Sym-H of -100 nT just after the first sharp decline in the AL index. The magnetic storm began just after 0200 UT and most likely resulted from a shock in the solar wind at about 0130 UT. The vertical lines indicate that the omega bands occur before and during the recovery phase of the magnetic storm.

The next three panels in Figure 3 show the IMF *Bx, By*, and *Bz* components in GSM coordinates from both Wind (blue curves) at about (198,-18,-24) Re GSM and Geotail (black curves) at about (-2,-25,-14) Re GSM. The IMF data from Wind and Geotail have been propagated from their locations to a nominal bow shock at (17, 0, 0) GSM using the *Weimer et al.*, [2003; 2004] technique. These data show that the *Bx* components remain negative and the *By* components are generally positive from 0400 to 1100 UT except for several brief positive and negative excursions, respectively. The *Bz* component starts at about -11 nT at 0400 UT and decreases to about –15 nT by 0500 UT, then sharply rotates to about 13 nT at 0515 UT at about the same time as the AL index sharply decreases. At 0600 UT the *Bz* component gradually drops below zero to -10 nT then rises back to an average of about 8 nT just before 0700 UT when the AL index sharply decreases a second time.

The bottom two panels of **Figure 3** show the solar wind speed and density from the Wind and Geotail spacecraft. The speed is about 500 km/s from 0400 UT to about 0500 UT after which it increases to 600 km/s by 0600 UT and remains at about that value from about 0600 to 1100 UT. During this time period both the *Vy* component and *Vz* components are steady. The densities measured by Wind and Geotail are initially very different. The Wind spacecraft measures a density of about 11 $\#cm^{-3}$ that peaks at about 20 $\#cm^{-3}$, but the Geotail spacecraft records a value of about 5 $\#cm^{-3}$. It is unclear why the Wind and Geotail density values disagree. The two times series converge to 8 $\#cm^{-3}$ by about 0615 UT, remaining well correlated and relatively steady between 8 and 10 $\#cm^{-3}$ until 11 UT.

In addition to observing the omega bands, the ASIs at ATHA, TPAS, GILL, and KAPU record several periods of pulsating aurora between 0430 UT and 1050 UT. For the ATHA ASI in the west we find a period of about 10.8 s, for TPAS we find a period of 12.4 s, for GILL we get a period of 21.6 s, and at KAPU the eastern most station the period is 18.8 s.

Complimentary to the images provided by ASIs, ground magnetometer data are available from 78 stations scattered over North America and Greenland. Using the *X* and *Y* magnetic field components (geographic north and east, respectively) from the magnetometers, we derive the SECs and overlay these on the auroral images. The current amplitudes (vertical currents) are shown in the top panel of **Figure 4** for the large omega bands observed at 0930 UT. We selected this time because the spatial resolution of the SECs is low and the analysis is, therefore, more informative for events in which the scale of the omega bands is large. The red “+s” and blue squares indicate upward and downward currents, respectively. The key is given in the lower left corner. The red line on the left side of the image indicates local midnight. The blue squares extending from Alaska across Canada to Hudson Bay (~60° Glat, ~270° Glon) reveal where the region 1 current flows into the ionosphere and the red crosses below the blue reveal where the region 2 current flows out. The poleward edge of the omega bands typically lies within 1.5° in latitude of the boundary between the region 1 and region 2 current systems. The largest upward region 2 current corresponds to the brightest omega band form (observed by ATHA) at 0930 UT. Thus the location of the omega bands that we observe is consistent with that previously reported by *Opgenoorth et al*. [1983], *Amm* [1996], and *Amm et al*. [2005].

The key in the lower left corner in the top panel of Figure 4 indicates that the upward SECs areabout 10,000 Amps and the downward SECs are approximately 20,000 Amps in the vicinity of the omega bands. If we roughly convert these currents into current densities by dividing by the area around each SEC pole, then we obtain currents of approximately 0.3 $\mu A/m^2$ upward and 0.7 $\mu A/m^2$ downward. These values are a factor of 6 to 3 lower than those estimates of ±1.7 $\mu A/m^2$ in *Yamamoto et al.* [1993].

The equivalent ionospheric current vectors are plotted in yellow in the lower panel of **Figure 4**. The yellow dots show the locations at which the currents are derived. The key is given in the lower left corner. The equivalent currents in the lower panel cross from the dayside over the Northwest Passage into Hudson Bay (~60° Glat, ~270° Glon), then turn and diverge both west (~53° Glat, ~260° Glon) and eastward (~53° Glat, ~280° Glon) at the southern end of Hudson Bay. The omega bands in the image are located in the westward electrojet, consistent with the analysis of *Opgenoorth et al*. [1983]. *Opgenoorth et al*. [1983] found in the vicinity of the omega bands the equivalent currents point on average from east to west, but turn northward at the eastern edge of the omega and then curl back southward on the western edge of the omega.

We are fortunate to have some Super Dual Auroral Radar Network (SuperDARN) [*Chisham et al*., 2007] ionospheric flow data available throughout the entire omega band event at 2 min temporal resolution. Observations from the SuperDARN (not shown) provide an indication of the prevailing ionospheric flows. The omega bands appear to be located in a region of eastward ionospheric flow, consistent with the direction of the omega band motion and their location in the westward equivalent ionospheric currents. The flow speeds measured by SuperDARN (300-400 m/s) are generally less than the speed determined from the auroral images of the omega bands between 0854 and 0930 UT (500-600 m/s), however, unfavorable radar beam orientations, and the likely E-region origin of the radar scatter in the vicinity of the omega bands, places considerable uncertainty on these values. The uncertainty in the E-region speed is largely due to the possibility of ionospheric irregularities being formed by the two-stream instability mechanism within the ionosphere [*Milan et al.,* 1997]. The difference in the speeds might suggest that the omega bands are not moving at the convection speed of the ionosphere, but the uncertainty in the inferred speed of the ionosphere is too large to validate such a conclusion.

In addition to inferring the SECs from the magnetometer data, we also analyzed the low frequency power in the *X* and *Y* components of the magnetic field measured in the vicinity of the ASIs at ATHA and TPAS. Previous studies [*Saito* 1978; *André and Baumjohann,* 1982] indicate that Ps6 pulsations (>600 s period or <1.7 mHz) are commonly observed in ground magnetometer data in association with omega bands. **Figure 5** shows the *Bx* components from 8 different auroral zone magnetometers including those at ATHA and TPAS. None of these stations show what would be considered more than a couple of pulsations with periods in the Ps6 range (5 to 40 min) and dynamic power spectra for each station do not display clear spectral peaks in the Ps6 frequency range. The *By* and *Bz* components (not shown) display similar results.

André and Baumjohann [1982] demonstrated for an event on February 1977 that the Ps6 pulsations are due to a regular amplitude and wavelength in the Hall currents associated with the omega bands in the auroral oval. In our event, the spacing of the omega bands is non-uniform, which is consistent with the absence of Ps6 pulsations.

In addition to ground based imagers, magnetometers, and radar, data from space-based magnetometers and plasma instruments are available from both the THEMIS mission and 4 GOES spacecraft. **Figure 6** is a plot of the XY GSM positions of the THEMIS, and GOES spacecraft during 4 of the 5 omega band intervals when these GOES spacecraft are near the mapped location of the omega bands. The corresponding interval number is given in the upper left corner. The brown zigzag curves shown near -10 Re down tail and close to the Sun-Earth line give the approximate location of the mapped poleward edge of the omega bands shown for 0439 UT in **Panel A**, 0629 UT in **Panel C**, 0651 UT in **Panel D**, and 0939 UT in **Panel E** of **Figure 2**. These curves have been traced from the ionosphere to the GSM equatorial plane along field lines using the *Tsyganenko* 1996 (T96) [*Tsyganenko*, 1996] model with the appropriate solar wind and Dst index inputs. We have arbitrarily selected the T96 model to trace the omega bands from the ionosphere to the tail. During the extreme geomagnetic conditions associated with the omega band intervals none of the available Tysganenko magnetic field models would be appropriate and the tracing of the omega bands into the tail is meant to indicate roughly where the omega bands could be located in the magnetotail. The magnetotail location of the omega bands suggests that the omega bands present in the tail during the first, third, and fourth time intervals are near the local time location of GOES 12 and 13. Furthermore, the magnetotail location of the lowest latitude portions of the poleward edge of the omega bands is located just inside of geosynchronous orbit, while the higher latitude portions map beyond or well beyond geosynchronous orbit.

Figure 7 shows the magnetic field and plasma data from the THEMIS spacecraft during the five omega band periods. The top three panels show the *Bx*, *By*, and *Bz* GSM components of the magnetic field from THC (green), THD (gray), and THE (blue) spacecraft. Data from THB and THA are not shown because they provide no additional information. As in **Figure 3**, the gray patches indicate the omega band periods. The flow and density moments measured at the three THEMIS spacecraft are given in the fourth through seventh panels. A number of observations can be drawn from these data.

The first interval of omega bands begins at about 0439 to 0443 UT when the THEMIS spacecraft are about an hour west in local time from the mapped locations of the auroral features and most likely the closest the THEMIS spacecraft ever get to the magnetotail location of the 5 omega bands groups. Prior to this interval THC records earthward high speed flows with a peak of ~140 km/s at about 0423 UT and moderate speed flows of about 80 km/s at about 0434 UT. It is not clear that these flows are associated with the streamer in Panel A of **Figure 2**.

The third omega band interval from 0611 to 0631 UT occurs just after a series of large fluctuations from 0524 to 0610 UT in the THC, THD, and THE FGM magnetic field vectors and just after a moderate tailward flow of -110 km/s at 0604 UT at THC. The magnetic field fluctuations occur after a sharp drop in the AL index at 0513 UT and could be related to high speed flows in the tail and/or substorm activity, but no auroral substorm was identified in the all sky images.

At the beginning of the fourth omega band interval at 0645 UT the flow is quiet and steady, but during the interval at about 0658 UT the *Vy* component at THC, THD, and THE peaks around 130 km/s and the density drops below 0.5 #cm^{-3}. During this time period the THEMS spacecraft and the equatorial mapping of the omega bands are separated by about 4 R_E in the YGSM direction. The magnetic field at all three THEMIS spacecraft is between -35 and -60 nT, which suggests that the spacecraft are either very close to or in the southern lobe. At about 0650 UT the flows increase, the magnetic field dipolarizes, and shortly afterward the omega bands shrink and disappear. For about 1.25 hours there are a significant number of erratic high speed flows both earthward and tailward at THC, THD, and THE. For this specific period of THEMIS flow data, *Du et al.* [2011] associated some of the flows between about 0714 and 0724 UT with the plasma sheet boundary layer because the ion density, ion temperature, and ion/electron spectrum displayed characteristics of the outer plasma sheet boundary layer. Plasma sheet boundary layer flows could indicate the presence of high sped flows in the plasma sheet, but not necessarily. After these flows begin to decrease the omega bands begin to reappear during the fifth interval from 0826 to 1054 UT, but by this UT time the local time of the omega bands is several hours from the local time of the THEMIS spacecraft. At the end of the fifth omega band interval high speed flows again appear in Vx and Vy. The important observations to take away from the THEMIS data are a number of high speed flows are observed in the magnetotail to the duskside of the field line mapped location of the omega bands.

Although the THEMIS spacecraft data were obtained duskward of the mapped positions of the omega bands in the equatorial plane, **Figure 6** shows that the geosynchronous GOES spacecraft were located in approximately the same local time sector as well as to the dusk and dawn of these locations, although closer to earth. During the first omega band interval GOES 13 was approximately in the same local time region as the THEMIS spacecraft and by the fourth interval GOES 11 was in the same local time region as the THEMIS spacecraft. During the second interval, not shown in **Figure 6**, the omega bands were close to the local time of GOES 10. **Figures 8** and **9** show the eastward and poleward components of the magnetic field from GOES 10-13. The panels from top to bottom are in the order of the GOES spacecraft from dusk to dawn (see **Figure 6**). At approximately 0529 and 0650 UT there are sharp changes in the eastward component at GOES 11. At the times of these sharp changes in the eastward component, the poleward component at GOES 11 (see **Figure 9**) also increases sharply, consistent with dipolarization events in the magnetotail. Dipolarization is also observed at about 0708 UT at GOES 13, which is about 7 Re to the east. If the dipolarizations at GOES 11 and GOES 13 are part of the same dipolarization front, then the azimuthal speed of propagation from GOES 11 to GOES 13 is about 41 km/s, which is consistent with azimuthal speeds of dipolarization fronts observed at THEMIS [*Runov et al.,* 2009]. Despite the close conjugate location of the omega bands in the magnetotail and the GOES spacecraft there is no clear one to one relationship between the omega bands and the changes in any of the GOES magnetic field components.

Arguably the most interesting features of **Figure 8** are the pulsation packets observed at all 4 GOES spacecraft after 0830 UT during the last omega band interval. The amplitude of these approximately 5.6 mHz pulsations are largest in the eastward component at GOES 10 and 12, but they are also present in the northward component. The 5.6 mHz pulsations are most likely magnetic field line resonances in the Pc 5 band. The GOES 12 spacecraft are located on field line with an L shell of approximately 7.1 and *Water et al.* [1995; 1996] reports that the field line resonance for an L shell of about 7 to be on the order of 4 mHz. A close look at the GOES 13 eastward component shows, in addition to the set of low frequency pulsations (5.6 mHz), a packet of higher frequency pulsations (13.9 mHz) in the Pc4 band from about 0944 – 0950 UT. The higher frequency pulsations at 16.7 mHz are also present in the GOES 11 spacecraft data from about 0932 to 0948 UT, but the lower frequency pulsations are not. Table 2 summarizes the results of power spectral analysis of the eastward component for different pulsation intervals. The frequencies of the pulsations observed at the GOES spacecraft are lower than those observed in the pulsating aurora (between 46 and 93 mHz), which starts before 03 UT, and higher than typical Ps6 pulsations. During the pulsation intervals, GOES 13, GOES 12, and GOES 10 are nearly conjugate to the ground magnetometers TPAS, SNKQ, and NAIN, respectively. All three ground magnetometers record small amplitude Pc5 pulsations with about the same period recorded by the GOES 13, 12, and 10 magnetometers.

Figure 8 shows four packets of pulsations in the GOES 12 and 10 eastward magnetometer data at about 0840, 0900, 0940, and 1025 UT. The packets start about 19 to 51 s earlier at GOES 10 than GOES 12 depending on the packet. The packets at 0840, 0940, 1025 UT appear to be correlated with sharp changes in the H component of multiple ground magnetometers in Alaska at 0835 and 0937 UT and sharp changes in the H component in central Canada at 1012 UT. Sharp changes in the H component have been associated with plasma sheet high speed flows in prior studies [*Runov et al.*, 2010], but we cannot clearly demonstrate a one to one correlation between the sharp change in the H component and high speed flows in the tail because we do not have flow data in the tail at the corresponding conjugate location.

Now we turn to the GOES spacecraft particle data. **Figure 10** shows the electron and proton data from the four GOES spacecraft. The top four panels display the proton data for the 0.8 to 4 MeV protons and the bottom four panels present the electron data. The panels from top to bottom within each group are in the order of the GOES spacecraft positions from dusk to dawn and the gray patches indicate each omega band event. The proton data are from the lowest available energy range from the Energetic Particle Sensor (EPS) on GOES 10-12 and the Energetic Proton, Electron and Alpha Detectors (EPEAD) on GOES 13, which outside of solar energetic particle events continuously observes a trapped proton population [*Green et al.,* 2004]. The higher energy channels are not plotted here because they do not show any clear changes during the interval plotted and they are too insensitive to observe the trapped population at these higher energies, if it is present. The electron data from GOES 10-12 consist of the >800 keV electrons from EPS. The electron data from GOES 13 are from telescope 9 of MAGED (pitch angles near 65°) over an energy range from 30 keV to 600 keV.

The GOES 10 proton data in the fourth panel of **Figure 10** shows an increase in the proton fluxes that peaks at about 0454 UT. Similar peaks occur in the GOES 12 proton data at about 0456 UT and GOES 13 proton data at about 0457 UT, but none is observed at GOES 11. The GOES 11 proton data in the first panel of the **Figure 10** shows an injection of protons at about 0525 UT. No concurrent enhancement is observed at the other GOES spacecraft. The same statement can be made for the proton flux enhancement at GOES 10 starting at about 0600 UT. The GOES 13 data in the second panel of **Figure 10** shows a gradual increase in the proton fluxes starting at around 0645 UT and GOES 11 displays a sharp increase at 0649 UT. Increases in the proton are also evident at GOES 12 (~0701 UT) and 10 (0705 UT). We conclude from this discussion that multiple enhancements are most likely related to multiple injections localized in azimuth into geosynchronous orbit, but there is no one to one correlation with the omega bands.

The proton data from the GOES 10-13 spacecraft provide some information on particle injections at ~0525 UT and ~0649 UT, but the interpretation of the electron data from GOES 10, 11, and 12 is less straightforward. The GOES 11 electron fluxes in the fifth panel decrease by about 2 orders of magnitude just before 0500 UT and small, possibly related, decreases (without recovery) are apparent at GOES 12 (Panel 7) at about 0511 UT and GOES 10 (Panel 8) at about 0520 UT. GOES 13 in Panel 6, on the other hand, shows increases in the 4 lowest energy channels at about 0525 UT and a clear dispersionless injection at 0657 UT related to the dispolarization discussed in relation to the magnetic field data. Weak electron injections are also visible at GOES 12 and 10 at about 0708 UT and 0740 UT, respectively. Based on the electron enhancements we reach the same conclusion as we did with the proton fluxes, which is that multiple, localized injections have occurred at geosynchronous orbit.

Finally, the sharp decrease in the electron and proton fluxes from GOES 13 starting at about 0845 UT and lasting until about 0900 UT occurs when GOES 13 enters the northern lobe region. This sharp decrease also corresponds to a dip down to –40 nT at 0859 UT in the eastward component of GOES 13. **Figure 11** supports that statement. This figure displays the TPAS ASI observations in a keogram format in the top panel, the GOES 13 electron fluxes for several energy channels in the middle panel, and the GOES 13 earthward (black) and eastward (blue) magnetic field components in the bottom panel. The top panel displays a keogram of the TPAS ASIs extracted at the longitude of the GOES 13 foot point as determined from magnetic field line trace using the T01 magnetic field model with the appropriate input conditions. The top and bottom of the keogram have been cropped above 65° GLat and below about 44° GLat, respectively. In Figure 11we have mapped the spacecraft location to the ionosphere (black curve in the top panel) using the T01 model because with this model the foot point crosses through a dark portion of the keogram at about 0855 to 0910 UT at roughly the time when GOES 13 is in the lobe region in the bottom two panels. The foot point determined with T89 and T96 magnetic field models put the foot point at a lower latitude that remains within the auroral oval for the entire time period shown in **Figure 11**. The period where the foot point enters the region of reduced emissions is well correlated with the periods when the electrons flux sharply decrease as it should in the lobe (second panel), the earthward component of the magnetic field dramatically increases as expected in the lobe (bottom panel), and the eastward component of the magnetic field become quite negative. We also note that the significant increases in the electron flux at both 0525 UT and 0657 UT are well correlated with increases in the auroral emissions in the keogram.

4. Discussion

We have presented a number of data sets from both ground and space based observatories for the five different omega band intervals observed on March 9th, 2008. In this section we use these different data sets to test the validity of two of the more widely accepted generation mechanisms for producing omega bands. It has been suggested that omega bands correspond to waves resulting from the Kelvin-Helmholtz instability arising in sheared flows in the equatorial regions of the tail and, alternatively, that omega bands form as a direct consequence of auroral streamer activity /high speed flows in the magnetotail.

Rostoker and Samson [1984] proposed that the Kelvin-Helmholtz instability in the magnetotail could produce omega bands in the aurora. They hypothesized that large-scale waves develop through a velocity shear at the interface between the central plasma sheet (CPS) and the low latitude boundary layer/boundary layer plasma sheet (LLBL/BLPS). **Figure 2** of *Rostoker and Samson* [1984] suggests that omega bands form at the interface LLBL/BLPS and the CPS between about 00 MLT and 3 MLT and between about 10 R_e and 37 R_e downtail. Such waves would map to the ionosphere where they would create the omega bands. *Rostoker and Samson* [1984] believed that the horizontal scale size and azimuthal velocities found in ground-based measurements can be explained by variations in the shear flow and width of the regions where the instability occurs. However, as we have shown, the omega bands map (with the T96 model) closer to the Earth than the LLBL/BLPS, at about the location of the inner edge of the plasma sheet [*Jiang*, 2013]. *Pulkkinen et al*. [1991] came to the same conclusion using the Tsyganenko 1989 model [*Tsyganenko*, 1989]. Although *Rostoker and Samson* [1984] suggest that omega bands form at the interface of the LLBL/BLPS and the CPS, one might alternatively consider a flow shear at the inner edge of the plasma sheet as the source region for omega bands. In that case, one would expect to measure a shear in the *Vy* component of the flow in that region. The closest spacecraft to the inner edge of the plasma sheet that provide flow-shear measurements are THD and THE, but these spacecraft are quite far from the local time at which the omega bands (**Figure 6**) are observed. Despite the large azimuthal separation, we examine the possibility of a link between the conditions at the spacecraft and the omega bands for completeness. In **Figure 12** we have plotted the *Vx* (1^{st} panel) and *Vy* (2^{nd} panel) GSM components from THD and THE, the *Bz* GSM component (3^{rd} panel), and in the last two panels we have plotted the quiver plots of the *Vx* and *Vy* components from THD and THE that have been filtered with a Pc4 pass band filter. The Pc4 pass band filter was arbitrarily selected to best show the general shape of the flows. The second panel in **Figure 12** shows that just prior to the second, third, fourth, and fifth omega band events there are no strong *Vy* flow shears and there is no clear relationship between the *Vy* values and the omega band intervals. The only strong *Vy* flow shears worth noting occur during the first omega band interval at about 0443UT when there are *Vy* flows on the order of –75 km/s followed by flows of the order of 100 km/s, however, THD and THE are approximately 4 Re away from the omega bands in the YGSM direction. As an additional means of examining this flow shear mechanism we have considered the width of the flow shear as it would appear field line mapped to the ionosphere. If we assume that the flow shear recorded at THE and THD from about 0443 UT to about 0449 UT passes over the two spacecraft and map the location of shear flow to the ionosphere at these two times, then the longitudinal width of the flow shear would be about 1°, which is similar to the wavelength and amplitude of a single small omega band (~1-2°), but the latitudinal difference in the mapped location is 0.03°. However, the during the third omega band interval there are several omega bands and the longitudinal width is about 5°. From this crude test we can say that flow shears in the inner plasma sheet are present and may have the potential for producing omega bands of the size observed in the ionosphere, but the size of the flow shear and the local time of the flow shear do not support the all sky image observations.

Prior to the second, third, and forth omega band intervals in **Figure 12** there are also no strong shear flows or dawnward flows and prior to and during the fifth omega band interval the bulk of the *Vy* flows are in the positive (duskward) direction (i.e., no obvious shears). These flow observations do not support the presence of the Kelvin-Helmholtz instability; however, the large separation between the THEMIS spacecraft and the field line mapped location of the omega bands prevents us from refuting the theory that Kelvin-Helmholtz instabilities could produce omega bands. All that we can conclude is that there is no evidence of the Kelvin-Helmholtz instability in the available the flow data.

There are some ASI observations that do support the flow shear theory. If flow shears are the source of omega bands, then the omega bands would appear to grow out of the auroral oval.

There are a total of 26 omega bands observed over all 5 intervals and we are able to see the development of 10 of these omega bands from the auroral oval. Some of these evolve out of the auroral oval while some form from activity within the auroral oval. However, none of the omega bands continue to evolve into torch like structures as observed in the model of Yamamoto et al. [1993].

The remaining mechanism proposed for the generation of omega bands formation we will investigate is auroral streamer activity. For this mechanism a spatially, quasi-periodic perturbation of the surface separating the dipole-like and tail-like magnetic field lines occurs in the midnight sector in the near-earth magnetotail region [*Henderson et al*., 2002; Henderson, 2009; 2012]. *Henderson et al.* [2002] and *Henderson* [2009] suggested that earthward directed flows in the magnetotail could be responsible for perturbing the surface separating the dipole-like and tail-like magnetic field lines. This mechanism was proposed because multiple Viking auroral images showed approximately north-south streamers that evolve into omega bands during substorms. Numerous studies have demonstrated a link between the north-south streamers and high speed, azimuthally confined, earthward flows in the magnetotail [*Henderson et al.*, 1994; 1998; *Zesta et al*., 2000; *Nishimura et al*., 2010]. It is these high speed flows that transport mass and momentum into the inner magnetosphere [*Angelopoulos et al*., 1994] and perturb the transition region between dipole-like and tail-like magnetic field lines. In **Figure 2** we showed examples at 0428 UT and 0620 UT in which the ASIs recorded north-south streamers that developed into the first and third interval of omega bands. North-south streamers were not observed to develop into omega bands before the second and fifth omega band intervals, possibly because those omega bands developed outside the region of ASI images and drifted into the field of view. Before 0428 UT, THC measured earthward flow (*Vx* in **Figure 7**) of about 140 km/s at about 0423 UT at THC, but not at THD and THE. This suggests that the high speed flow channels were present over spatially limited portions of the tail and that the failure of THD and THE to detect the flows was either because the flow channel was azimuthally narrow or that the flows did not penetrate into the inner magnetosphere. When we use the T96 or T89 magnetic field models to trace to the location of the three THEMIS spacecraft to the ionosphere we find that the foot point for THC is located just to the dawn side of the north-south streamer in the first panel of **Figure 2**, THD is located in the streamer, and THE is just to the duskside of the streamer. THD did not detect any high speed flows whereas THC did, but this inconsistency is within the uncertainty of the magnetic mapping. If we repeat the same field line tracing process and instead use the T01 magnetic field model, then the foot point for THC maps a few degrees to the west of the streamer, the foot point for THD maps 5° to the west, and the foot point for THE is located 8° to the west. By using the different magnetic field models we confirm that magnetic field line tracing is uncertain within a few degrees and that the location of the foot points is uncertain on the scale of the structures of interest. The variations from one spacecraft to another nearby spacecraft confirms the presence of a longitudinally narrow, earthward directed flow channel, and mapping shows that the foot points of the spacecraft fall roughly in the region in which omega bands develop.

The streamer in the fourth panel of **Figure 2** at 0620 does not appear to be associated with high speed earthward flows recorded by any of the THEMIS spacecraft. If we trace the location of all three THEMIS spacecraft to the ionosphere using the T89, T96, and T01 magnetic field models, the foot points of the spacecraft for all three models are located 5° or more to the west of the streamer in the mosaic in the fourth panel of **Figure 2**. This finding leads us to believe the

THEMIS spacecraft are not in the appropriate location to record a high speed flow in the tail that could be associated with the auroral north-south streamer. All we can say about the fourth panel in Figure 2 is that fast earthward flows are probably present somewhere in the tail other than where measurements are available and such flows could perturb the inner edge of the plasma sheet to cause the omega bands as proposed by *Henderson* [2009].

Prior to the fourth omega band intervals no north-south streamers were clearly observed in the ASI mosaics and no high speed earth flows in the magnetotail were measured at THC, THD, and THE during the interval of interest. However, GOES 11 and 13 spacecraft indicate that activity was present in the inner magnetosphere that may have been associated with perturbation of the inner plasma sheet boundary. GOES 11 does record the injection of 0.8 to 4.0 MeV protons at the beginning of the fourth interval and a dipolarization in the middle of the interval. GOES 13 also shows a dispersionless injection of 30-600 keV electrons in the middle of the fourth interval, which has been associated with high speed earthward flows in the tail [*Zesta et al.*, 2000].

In the fifth interval, no north-south streamer appears prior to the development of the omega bands, but no ASI data showing the full development of these omega bands were available. However, a significant period of high speed tailward and earthward flows was observed at THC, THD, and THE from 0658 UT to 0825 UT, which is between the fourth and fifth omega band intervals. The standard AL index and many of the ground magnetometers in Alaska and Northwestern Canada also display sharp decreases in the H component of the magnetic field. These sharp changes have been previously associated with high speed earthward flows. Furthermore, a short ~2 min burst of high speed flows occurs at 0948 UT and a sharp increase in the density occurs at all three spacecraft between 0942 and about 1000 UT just before the interruption in the train of omega bands during the fifth interval between 0950 UT and 1011 UT.

Whether these flows are associated with the fifth group of omega bands is unclear, but they may well have perturbed the inner plasma sheet boundary. These high speed flows during the fifth omega band interval may also explain the 5.6 mHz pulsations observed by both the GOES spacecraft and near conjugate ground magnetometers. The high speed flows when they reach the inner edge of the plasma sheet could produce fast mode waves. Fast mode waves can propagate through the inner magnetosphere and can produce the field line resonances observed at the GOES 10 and 12 spacecraft. This process is similar to the propagation of compressional waves produced at the magnetopause generated by sudden impulses in the solar wind [*Chi et al.,* 2001]. However, some caution should be exercised when considering the high speed flows because the THEMIS FGM *Bx* component indicates that THC, THD, and THE are in the magnetotail lobes and the high speed flows may be associated with the plasma sheet boundary layer, a conclusion also reached by *Du et al.* [2011]. Unfortunately, the GOES spacecraft do not provide any additional information to suggest that the inner plasma sheet boundary was perturbed. During the fifth interval the omega bands map farther down the tail at about 8 Re and the GOES spacecraft may not have been able to measure any possible inner plasma sheet boundary perturbations.

If high speed flows are the generation mechanism for omega bands, then the duration of the high speed flows should be on the order of the duration of the omega bands. The typical duration of these high speed flows is on the order of 1 to 10 min [*Angeloupoulos et al.,* 1994].and in this study the high speed flow observed by THEMIS lasted between 3 and 3.5 min. Using the ASIs of the omega bands we find the life time of those omega bands we could follow from their development to their conclusion varied between 1.5 to 17 min, which is within a factor of 2 of the Angelopoulos et al. [1994] study. However, two omega bands during the fifth omega band interval, which we were unable to see develop, had life times greater than 22 min and 28 min.

Furthermore, if the high speed flows in the tail are the source of the omega bands, then we should see the north south arcs, which are the ionospheric projection of the high speed flows, develop into the omega bands. We found a total of 26 omega bands observed over all 5 intervals and we are unable to see the development of 11 of these omega bands. Five of the omega bands appear to develop from north southern streamers, but 10 of the omega bands appear to develop out of the equatorward portion of the auroral oval. We note that the 5 omega bands that evolve from streamers typically have amplitudes of 1° to 4.5° with mean of 3°. Furthermore, there are a number of north south streamers in the midnight sector between 0428 UT and 1100 UT that do not develop into omega bands. Those omega bands that grow out of the equatorward portion of the auroral oval had a mean amplitude of 1° and never exceed an amplitude of 3°. Finally, none of these develop into torches as observed in the model of Yamamoto et al. [1993].

The suggestion that high speed earthward flows causes omega bands requires that the inner edge of the plasma sheet develop surface undulations. Narrow flow channels of the sort required have been found in global magnetohydrodynamic (MHD) simulations of a substorm event that occurred on August 25, 2013, which does not show any omega bands in the ASIs, and in other reported MHD simulations [*El-Aloui et al*., 2009; 2013]. **Figure 13**, extracted from the simulation, shows how such flows can corrugate the inner edge of the plasma sheet. The results shown here were obtained from a global MHD model developed by *Raeder et al.* [1998] and *El-Alaoui et al*. [2001]. Shown in **Figure 13** are four different time periods (the time is given in the upper left corner of each panel) where the data are obtained from the central plasma sheet. Each panel shows the flow as purple vectors with key to the scale in the upper right, pressure contours (gray curves), and the magnetic perturbation about the mean δBz (color) with a color bar on the right side of each panel in **Figure 13**. In all four panels high speed flows are coming into the inner magnetosphere in both the pre and post might sectors. In the top right panel a divot in the pressure contours forms at about (-11, -2) Re (marked with the yellow segment) and appears to drift to the dawnside, which is shown with the green line, of the magnetosphere as time passes. The divot drift has a speed in the range of 7 to 12 km/s. The large omega bands during the fifth interval have a speed in the magnetotail of about 23 km/s when we magnetic field line trace the omega bands with the T96 model and follow the motion of the omega bands in the tail. Similar results were obtained from the T89 and T01 models. At 0550 UT in the MHD simulation several other divots occur on the boundary of the inner magnetosphere and the shape of the pressure contour looks similar to the magnetic field line traces of the omega bands displayed in the lower panels of **Figure 6**. Furthermore, the wavelength of the ripple in the pressure contour in **Figure 13** is similar to the wavelength of the field line trace of the omega bands in **Figure 6** and on the order of 1 to 2 Re. We believe the results from the MHD model suggest that the earthward high speed flows could be the source of the perturbations at the inner edge of the plasma sheet that lead to the omega bands.

We have presented evidence from a variety of ground and space based instrumentation showing that high speed flows occurred in the near magnetotail between about 0400 UT and 1100 UT on March 9th, 2008. Even though the measured high speed flows were not at local times that mapped to the omega bands, it seems probable that such flows were present over a broad range of local times and we believe that the bulk of the omega bands were produced by earthward high speed flows. **Figure 14** presents our interpretation of the formation of the omega bands. In the top left panel a high speed earthward flow is present in the tail resulting from an x-line in the mid tail, which produces the divot in the pressure iso-contours that were observed in the MHD model. The pressure iso-contour divots in Figure 13 are on the order of 1 Re deep and

1 Re wide at about 10 Re down the magnetotail and caused by high speed earthward flows that are a few Re wide and several Re long. On the dawnside of the flow is a field aligned current out of the plasma sheet in to the ionosphere due to the velocity shear in the tail. On the duskside of the high speed flow is a field aligned current from the ionosphere to the plasma sheet. The upper left corner of the panel shows an expanded view of the auroral oval where the field aligned currents intersect the ionosphere on either side of a north-south streamer where north-south streamer is the auroral projection of the high speed earthward flow. Pedersen currents connect the downward and upward field aligned currents. The projection of the pressure iso-contour divots onto the ionosphere would be approximately 2 degree in longitude and about 0.3 degrees in latitude. These values were determined from both the MHD model used for Figure 13 and from the Tsyganenko magnetic field models. From the MHD simulations we get field align currents at the ionosphere of about 0.3 $\mu A/m^2$, which is similar to the values of 0.3 $\mu A/m^2$ and 0.7 $\mu A/m^2$ obtained from the spherical elementary currents method. We note also that the region 1 and region 2 currents are not equal to one another during the fifth omega band interval as suggested by *Janhunen and Huuskonen* [1993]. At some point reconnection in the x-line ends, but the high speed flows continue earthward as shown in the upper right panel. In the ionosphere a stretched omega band is present where the north south streamer used to be located and the field aligned currents are downward outside the omega band and upward within the omega band. Both the high speed flow in the tail and the omega band convect dawnward with the bulk plasma. The omega bands in the fifth omega band interval had a dawnward speed in the ionosphere, which equates to a value of about 23 km/s in the magnetotail. This dawnward speed of the omega bands was determined by field line tracing the omega bands to the equatorial plane for a series of images into the tail with the Tsyganenko models. In the two lower panels of Figure 14 the high

speed stream gradually shortens and the associated omega band decays as the flow and the omega band drift dawnward. As the earthward stream slows, the omega band disappears.

5. Conclusion

We have examined in detail a series of five omega band intervals that occurred on March 9th, 2008 between 0400 and 1100 UT. Data from a number of ground and space based instruments were available. We summarize the important findings here.

- Using the spherical elementary current method, we find that the brightest edge of the omega band lies at the boundary between the region1 and region 2 current systems.
- Pulsations were detected during the fifth omega band interval in the GOES spacecraft magnetometer data and 30-50 keV electron fluxes, and by ground magnetometers. The magnetic pulsations observed on the ground and in space appear to be independent of the omega bands, but the packets of pulsations appeared to be correlated with sharp changes in the H component of some ground magnetometers.
- Using the T96 magnetic field model we mapped the omega bands along field lines out into the magnetotail and found that they lie between 6 and 15 Re on the GSM equatorial plane.
- Four of the five omega band intervals examined here occurred during storm time conditions, extending over time intervals prior to and during substorm expansion within the storm. The geosynchronous magnetic fields were highly stretched throughout this period.

We surmise from our last point that omega bands are not systematically associated with the substorm recovery phase as previous studies have indicated. The first and third of the five periods of the omega bands evolved from north-south streamers. One of the intervals developed without evident association with streamers. The second omega band interval initiated outside the region imaged by the array. The fifth intervals of omega bands were initiated outside the region imaged by the array or developed or without evident association with streamers. Within the magnetic field model mapping error, the first streamer in the first interval maps to a region of high-speed (*Vx* = +140 km/s) earthward flow observed by THEMIS THC.

With the spacecraft data available we examined two possible generation mechanisms for the omega bands: the Kelvin-Helmholtz instability, and the high speed flows in the tail. THEMIS observations show some high speed flow shears in *Vy* that could be associated with the Kelvin-Helmholtz instability at THD and THE (closest to the omega bands). These *Vy* flows may indicate that shear flows were present but high speed *Vy* flow shears were not present during all the omega bands intervals. More than likely the THEMIS spacecraft were located too far to the west from the conjugate magnetospheric location of the omega bands.

The most probable mechanism for the formation of omega bands appears to be azimuthally localized high speed flows in the tail that distort magnetic shells when they reach the inner magnetosphere (**Figure 14**). Despite the availability of data from numerous spacecraft close to the regions to which the omega bands mapped, none was close enough to establish an unambiguous connection between high speed flows and omega bands. However, there was one case in which it was possible to link a flow observed in the tail to an auroral streamer that in turn linked to an omega band imaged by an ASI. This gives considerable support to the view that localized earthward flows are critical to the development of omega bands. And, although there were no direct links, data from the equatorial spacecraft established that numerous high speed earthward flows and magnetic dipolarizations occurred during the times when omega bands were observed. Additional support for the interpretation offered here is extracted from an MHD simulation of a substorm on August 2013. The simulation shows flow bursts that created corrugations of pressure surfaces that resembled the magnetotail mapped omega bands. Furthermore, the undulations from the MHD model also propagated dawnward just as did the omega bands in the all sky images with similar speeds. Clearly, more work is required to understand the source of auroral omega bands but this work makes it seem probable that azimuthally localized flows in the near tail are required to generate these structures.

Acknowledgements

To our regret Prof. Olaf Amm passed away during the writing of this manuscript and is included as coauthors for his invaluable help and discussion on the spherical elementary current system method and discussion related to his previous work on omega bands. We thank the many different groups operating magnetometer arrays for providing data for this study including: the Canadian Space Science Data Portal. The Canadian Space Science Data Portal is funded in part by the Canadian Space Agency, the Alberta Science and Research Authority, and the University of Alberta. The Canadian Magnetic Observatory Network (CANMON) is maintained and operated by the Geological Survey of Canada - http://gsc.nrcan.gc.ca/geomag. The Magnetometer Array for Cusp and Cleft Studies (MACCS) array is supported by US National Science Foundation grant ATM-0827903 to Augsburg College. We would like to would like to thank the following: Jürgen Matzka for calibrating the DTU magnetometers; M. J. Engebretson, D. Murr, and E.S. Steinmetz at Augsburg College; and the MACCS team. The Solar and Terrestrial Physics (STEP) magnetometer file storage is at Department of Earth and Planetary Physics, University of Tokyo and maintained by Dr. Kanji Hayashi (hayashi@grl.s.u-tokyo.ac.jp). This study was made possible by NASA THEMIS grant NAS5-02099 at UCLA. We also acknowledge NASA contract NAS5-02099 and V. Angelopoulos for use of data from the THEMIS Mission. Specifically: NSF for support of GIMNAST through grant AGS-1004736. We thank E. Donovan for use of the ASI data, and the CSA for logistical support in fielding and data retrieval from the GBO stations. The Alaska and Greenland portions of the GBO network are supported by NSF through grant 1004736. Dr. R. Redmon is supported by National Oceanic and Atmospheric Administration (NOAA). Dr. J.V. Rodriguez is supported by NASA grant NNX12AJ55G via Subaward 2090 G QA024 from UCLA to CIRES. We would also like to thank Dr. K.K. Khurana, Dr. R.L. McPherron, Dr. R.J. Strangeway, Dr. Emma Spanswck, Mr. E. Grimes, and Dr. R.J. Walker for their invaluable input.

References

·Akasofu, S.-I. and Kimball, D. S.(1964), The dynamics of the aurora, 1. Instabilities of the aurora, *J. Atmos. Terr. Phys*., **26**, 205.

·Amm, O. (1995), Direct determination of the local ionospheric Hall conductance distribution from two-dimensional electric and magnetic field data: Application of the method using models of typical ionospheric electrodynamic situations, J. Geophys. Res., 100, 24 173.

·Amm, O. (1996) Improved electrodynamic modeling of an omega band and analysis of its current system, *J. Geophys. Res*., **101**, 2677–2683.

·Amm, O., A. Aksnes, J. Stadsnes, N. Østgaard, R.R. Vondrak, G.A. Germany, G. Lu, and A. Viljanen (2005), Mesoscale ionospheric electrodynamics of omega bands determined from ground-based electromagnetic and satellite optical observations, *Ann. Geophys*., **23**, 325–342.

·Amm, O., and A. Viljanen (1999), Ionospheric disturbance magnetic field continuation from the ground to the ionosphere using spherical elementary current systems, *Earth Planets. Space.*, **51**, 431.

·André, D. and W. Baumjohann, W. (1982), Joint two-dimensional observations of ground magnetic and ionospheric electric fields associated with auroral currents, 5. Current system associated with eastward drifting omega bands, *J. Geophys*., **50**, 194.

·Angelopoulos, V. (2008), The THEMIS mission, *Space Sci. Rev*., **141**, 5-34, DOI: 10.1007/s11214-008-9336-1.

·Angelopoulos, V., C.F. Kennel, F.V. Coroniti, R. Pellat, M.G. Kivelson, R.J. Walker, C.T. Russell, W. Baumjohann, W.C. Feldman, and J.T. Gosling (1994), Statistical characteristics of bursty bulk flow events, *J. Geophys. Res*., **99**, 21,257–21,280, doi:10.1029/94JA01263.

·Auster, H.U., K.H. Glassmeier, W. Magnes, O. Aydogar, W. Baumjohann, D. Constantinescu, D. Fischer, K.H. Fornacon, E. Georgescu, P. Harvey, O. Hillenmaier, R. Kroth, M. Ludlam, Y. Narita, R. Nakamura, K. Okrafka, F. Plaschke, I. Richter, H. Schwarzl, B. Stoll, A. Valavanoglou, and M. Wiedemann (2008), The THEMS, Fluxgate Magnetometer, *Space Sci. Rev*., **141**, 235-264.

·Chisham, G., M. Lester, S. E. Milan, M. P. Freeman, W. A. Bristow, A. Grocott, K. A. McWilliams, J. M. Ruohoniemi, T. K. Yeoman, P. L. Dyson, R. A. Greenwald, T. Kikuchi and M. Pinnock, J. P. S. Rash, N. Sato, G. J. Sofko, J.-P. Villain, and A. D. M. Walker (2007), A decade of the Super Dual Auroral Radar Network (SuperDARN): scientific achievements, new techniques and future directions, Surv Geophys, 28, 33-109.

·Du, A. M., R. Nakamura, T.L. Zhang, E.V. Panov, W. Baumjohann, H. Luo, W.Y. Xu, Q.M. Lu, M. Volwerk, A. Retino, B. Zieger, V. Angelopoulos, K.-H. Glassmeier, J.P. McFadden, and D. Larson, (2011), Fast tailward flows in the plasma sheet boundary layer during a substorm on 9 March 2008: THEMIS observations, *J. Geophys. Res*., **116**, A03216, doi:10.1029/2010JA015969.

·El-Alaoui, M. (2001), Current disruption during November 24, 1996 substorm, *J. Geophys. Res*., **106**, 6229–6246, doi:10.1029/1999JA000260.

·El-Alaoui, M., M. Ashour-Abdalla, R. J. Walker, V. Peroomian, R. L. Richard, V. Angelopoulos, and A. Runov (2009), Substorm evolution as revealed by THEMIS satellites and a global MHD simulation, *J. Geophys. Res*., **114**, A08221, doi:10.1029/2009JA014133.

·El-Alaoui, M., R. L. Richard, M. Ashour-Abdalla, M. L. Goldstein, and R. J. Walker (2013), Dipolarization and turbulence in the plasma sheet during a substorm: THEMIS observations and global MHD simulations, *J. Geophys. Res. Space Physics*, **118**, doi:10.1002/2013JA019322.

·Elphinstone, R. D., D. J. Hearn, L. L. Cogger, J. S. Murphree, H. Singer, V. Sergeev, K. Mursula, D. M. Klumpar, G. D. Reeves, M. Johnson, S. Ohtani, T. A. Potemra, I. Sandahl, E. Nielsen, M. Persson, H. Opgenoorth, P. T. Newell, Y. I. Feldstein,. (1995), Observations in the vicinity of substorm onset: Implications for the substorm process, *J. Geophys. Res.,* 100(A5), 7937–7969, doi:10.1029/94JA02938.

·Engebretson, M.J., W.J. Hughes, J.L. Alford, E. Zesta, L.J. Cahill, Jr.,R.L. Arnoldy, and G.D. Reeves (1995), Magnetometer Array for Cusp and Cleft Studies Observations of the Spatial Extent of Broadband ULF Magnetic Pulsations at Cusp/Cleft Latitudes**,** *J. Geophys. Res.,* **100**, 19371.

·Green, J. C., T. G. Onsager, T. P. O'Brien, and D. N. Baker (2004), Testing loss mechanisms capable of rapidly depleting relativistic electron flux in the Earth's outer radiation belt, *J. Geophys. Res*., **109**, A12211, doi:10.1029/2004JA010579.

·Gustafsson, G., W. Baumjohann, and I. Iversen, I. (1981), Multi-method observations and modeling of the three-dimensional currents associates with a very strong Ps 6 event, *J. Geophys*., **49**, 138.

Hanser, F. A. (2011), EPS/HEPAD calibration and data handbook, Tech. Rep. GOESN-ENG-048D, Assurance Technology Corporation, Carlisle, Mass. [Available at http://www.ngdc.noaa.gov/stp/satellite/goes/documentation.html.]

·Henderson, M.G. (1994), Implications of Viking imager results for substorm models, Thesis (PhD), University of Calgary, Canada.

·Henderson, M.G. (2009), Observational evidence for an inside-out substorm onset scenario**,** *Ann. Geophys*., **27**, 2129–2140.

·Henderson, M. G. (2012), Auroral Substorms, Poleward Boundary Activations, Auroral Streamers, Omega Bands, and Onset Precursor Activity, in Auroral Phenomenology and Magnetospheric Processes: Earth And Other Planets Geophysical Monograph Series 197 (eds. A. Keiling, E. Donovan, F. Bagenal and T. Karlsson), American Geophysical Union, Washington, D. C. doi: 10.1029/2011GM001165.

·Henderson, M.G., J.S. Murphree, and G.D. Reeves (1994), The activation of the dusk-side and the formation of north-south aligned structures during substorms, in the Proceedings *of the Second International Conference on Substorms*, Fairbanks, Alaska, 37-42.

·Henderson, M.G., G.D. Reeves, and J.S. Murphree (1998), Are north-south aligned auroral structures an ionospheric manifestation of bursty bulk flows? *Geophys. Res. Lett.*, **25**, 3737-3740.

·Henderson, M.G., L. Kepko, H.E. Spence, M. Conners, J.B. Sigwarth, L.A. Frank, H.J. Singer, and Y. Yumoto (2002), The evolution of north-south aligned auroral forms into auroral torch structures: The generation of omega bands and Ps6 pulsations via flow bursts, Sixth international conference on substorms, ed. R.M. Winglee, University of Washington, Seattle, WA, 169174.

·Janhunen, P. and A. Huuskonen (1993) A numerical ionospheremagnetosphere coupling model with variable conductivities, *J. Geophys. Res*., **98**, 9519–9530.

·Jaynes, A. N., M. R. Lessard, J. V. Rodriguez, E. Donovan, T. M. Loto'aniu, and K. Rychert (2013), Pulsating auroral electron flux modulations in the equatorial magnetosphere, *J. Geophys. Res. Space Physics*, **118**, doi:10.1002/jgra.50434.

·Jian, L.K., C.T. Russell, and J..G. Luhmann (2011), Comparing solar Minimum 23/24 with historical solar wind records at 1 AU, *Solar Phys*., **274** (1-2), 321–344, doi:10.1007/s11207-011-9737-2.

·Jiang, F., (2013). The magnetospheric source of the pre-existing auroral arc., Dissertation University of California, Los Angeles: Geophysics and Space Physics.

·Jorgensen, A.M., H.E. Spence, T.J. Hughes, and D. McDiarmid (1999), A study of omega bands and Ps6 pulsations on the ground, at low altitude and at geostationary orbit, *J. Geophys. Res.*104, 14,706-14,715.

·Kawasaki, K. and G. Rostoker (1979), Perturbation magnetic fields and current systems associated with eastward drifting auroral structures, *J. Geophys. Res*., **84**, 1464.

·Lühr, H. and K. Schlegel (1994) Combined measurements of EISCAT and the EISCAT magnetometer cross to study bands, *J. Geophys. Res*., **99**, 8951.

·McFadden, J.P., C.W. Carlson, D. Larson, M. Ludham, R. Abiad, B. Elliott, P. Turin, M. Marckwordt, and V. Angelopoulos (2008), The THEMIS, ESA plasma instrument and In-flight Calibration, *Space Sci. Rev*. **141**, 277-302.

·Milan, S.E., T.K. Yeoman, M. Lester, E.C. Thomas, T.B. Jones (1997), Initial backscatter occurrence statistics from the CUTLASS HF radars, *Ann. Geophysicae*, **15**, 703-718.

·Mende, S.B., Harris, S.E., Frey, H.U., Angelopoulos, V., Russell, C.T., Donovan, E., Jackel, B., Greffen, M., and Peticolas, L.M. (2008), The THEMIS array of ground-based observatories for the study of auroral substorms, *Space Sci. Rev*., **141**, 357-387, doi: 10.1007/s11214-008-9380.

·Mravlag, E., Scourfield, M. W. J., Walker, A. D. M., Sutcliffe, P. R., and Nielsen, E. (1991), Simultaneous observations of omega band related phenomena in both hemispheres, *J. Atmos. Terr. Phys*., 53, 309.

·Nishimura, Y., L. Lyons, S. Zou, V. Angelopoulos, and S. B. Mende (2010), Substorm triggering by new plasma intrusion: THEMIS all-sky imager observations, *J. Geophys. Res*., **115**, A07222, doi:10.1029/2009JA015166.

·Nishimura, Y., L. R. Lyons, V. Angelopoulos, T. Kikuchi, S. Zou, and S. B. Mende (2011), Relations between multiple auroral streamers, pre-onset thin arc formation, and substorm auroral onset, *J. Geophys. Res*., **116**, A09214, doi:10.1029/2011JA016768.

·Oguti, T., S. Kokubun, K. Hayashi, K. Tsuruda, S. Machida, T. Kitamura, O. Saka, and T. Watanabe, An auroral torch structure as an activity center of pulsating aurora, *Can. J. Phys*., 59, 1056–1062, 1981.

·Onsager, T.G., R. Grubb, J. Kunches, L. Matheson, D. Speich, R. Zwickl, and H. Sauer (1996), Operational Uses of the GOES Energetic Particle Detectors. SPIE Conference Proceedings, Vol. 2812, p. 281-290, GOES-8 and Beyond, Edward R. Washwell.

·Opgenoorth, H. J., Oksman, J., Kaila, K. U., Nielsen, E., Baumjohann, W. (1983) Characteristics of eastward drifting omega bands in the morning sector aurora, *J. Geophys. Res*., **88**, 9171–9185.

·Opgenoorth, H. J., M. A. L. Persson, T. I. Pulkkinen, and R. J. Pellinen (1994), Recovery phase of magnetospheric substorms and its association with morning sector aurora, *J. Geophys. Res*., **99**, 4115–4129, doi:10.1029/93JA01502.

·Peroomian, V., S. Garg, and M. El-Alaoui (2014), An MHD simulation study of the dynamics of the 8–9 March 2008 CIR-/ HSS-driven geomagnetic storm, J. Geophys. Res. Space Physics, 119, 2990–3001, doi:10.1002/2013JA019294.

·Pu, Z. Y., A. Korth, Z. X. Chen, R. H. W. Friedel, Q. G. Zong, X. M. Wang, M. H. Wong, S. Y. Fu, and T. I. Pulkkinen (1997), MHD drift ballooning instability near the inner edge of the near-Earth plasma sheet, *J. Geophys. Res*., **102**(A7), 14,397–14,406.

·Pulkkinen, T.I., R.J. Pellinen, H.E.J. Koskinen, H.J. Opgenoorth, J.S. Murphree, V. Petrov, A. Zaitsev, and E. Friis-Christensen (1991), Auroral signatures of substorm recovery phase: A case study, in Magnetospheric Substorms, Geophys. Monogr. Ser., vol. 64, edited by J. R. Kan et al., pp. 333–342, AGU, Washington, D. C.

·Raeder, J., J. Berchem, and M. Ashour-Abdalla (1998), The geospace environment modeling grand challenge: Results from a global geospace circulation model, *J. Geophys. Res*., **103**, 14,787–14,798, doi:10.1029/98JA00014.

·Rostoker, G.J. C. Samson (1984), Can substorm expansive phase effects arid low frequency Pc magnetic pulsations be attributed to the same source mechanism? *Geophys. Res. Lett.*, ***11***, *271*.

·Roux, A., S. Perrant, A. Morane, P. Robert, A. Korth, G. Kremser, A. Pederson, R. Pellinen, and Z. Y. Pu (1991), Plasma sheet instability related to the westward traveling surge, *J. Geophys. Res.*, **96**(A10), 17,697–17,714.

·Runov, A., V. Angelopoulos, M. I. Sitnov, V. A. Sergeev, J. Bonnell, J. P. McFadden, D. Larson, K.-H. Glassmeier, and U. Auster (2009), THEMIS observations of an earthward-propagating dipolarization front, *Geophys. Res. Lett*., **36**, L14106, doi:10.1029/2009GL038980.

·Russell, C. T., P.J. Chi, D. J. Dearborn, Y.S. Ge, B. Kuo-Tiong, J.D. Means, D. R. Pierce, K.M. Rowe, R.C. Snare *(2008), THEMIS ground-based magnetometers, Space Sci. Rev., 141, 389–412.*

·Saito, T. (1977), Long-period irregular magnetic pulsation, Pi3, *Space Science Reviews*, **21**, 427-467, doi:10.1007/BF00173068.

·Saito, T. (1978), Long period irregular micropulsations, Pi 3, *Space Sci. Rev*., **21**, 427.

·Sergeev, V. A., K. Liou, C.-I. Meng, P. T. Newell, M. Brittnacher, G. Parks, and G. D. Reeves (1999), Development of auroral streamers in association with impulsive injections to the inner magnetotail, *Geophys. Res. Lett.*, **26**, 417.

·Sergeev, V., A. Runov, W. Baumjohann, R. Nakamura, T.L. Zhang, M. Volwerk, A. Balogh, H. Rème, J. A. Sauvaud, M. André and B. Klecker *(*2003*)*, Current sheet flapping motion and structure observed by Cluster, *Geophys. Res. Lett.*, 30*, 1327,* *doi:*10.1029/2002GL016500.

·Singer, H.J., L. Matheson, R. Grubb, A. Newman and S.D. Bouwer, Monitoring Space Weather with the GOES Magnetometers (1996), SPIE Conference Proceedings, Vol. 2812, p. 299-308, GOES-8 and Beyond, Edward R. Washwell, ed.

·Tagirov, V. (1993), Auroral torches: Results of optical observations, *J. Atmos. Terr. Phys*., **55**, 1775–1787.

·Toichi, T., and T. Miyazaki (1976), Flapping motions of the tail plasma sheet induced by the interplanetary magnetic field variations, *Planet Space Sci*., **24**, 147-159.

·Tsyganenko, N.A. (1989), Magnetospheric magnetic field model with a warped current sheet, *Planet. Space Sci*., **37**, 5.

·Tsyganenko, N.A.(2002a), A model of the near magnetosphere with a dawn-dusk asymmetry - 1. Mathematical Structure, *J. Geophys.Res*., **107**, A8, 10.1029/2001JA000219.

·Tsyganenko, N.A. (2002b), A model of the near magnetosphere with a dawn-dusk asymmetry - 2. Parameterization and fitting to observations, *J. Geophys. Res*., **107**, A7, 10.1029/2001JA000220.

·Tsyganenko, N.A., and D.P. Stern (1996), Modeling the Global Magnetic Field of the Large-Scale Birkeland Current Systems, *J. Geophys.Res*., **101**, 27187-27198.

·Vanhamäki, H., K. Kauristie, O. Amm, A. Senior, D. Lummerzheim, and S. Milan (2009), Electrodynamics of an omega-band as deduced from optical and magnetometer data, *Ann. Geophys.*, **27**, 3367–3385.

·Waters, C.L., J.C. Samson, E.F. Donovan (1995) , The temporal variation of the frequency of high latitude field line resonances, *J. Geophys.Res*., 100, 7987-7996.

·Waters, C.L., J.C. Samson, E.F. Donovan (1995) , Variation of plasmatrough density derived from magnetospheric field line resonces, *J. Geophys.Res*., 101, 24737-24745.

·*Wild, J. A.*, E.E. Woodfield,   E. Donovan, R.C. Fear, A. Grocott,   M. Lester,   A.N. Fazakerley,   E. Lucek,   Y. Khotyaintsev, M. Andre,   A. Kadokura,   K. Hosokawa, C. Carlson,   J.P. McFadden,   K.-H. Glassmeier, V. Angelopoulos, and G. Björnsson *(2011), Midnight sector observations of auroral omega bands, J. Geophys. Res., 116, A00I30, doi:*10.1029/2010JA015874.

·Weimer, D. R. (2004), Correction to ‘‘Predicting interplanetary magnetic field (IMF) propagation delay times using the minimum variance technique,’’ *J. Geophys. Res*., **109**, A12104, doi:10.1029/2004JA010691.

·Weimer, D.R., D.M. Ober, N.C. Maynard, M.R. Collier, D.J. McComas, N.F. Ness, C. W. Smith, and J. Watermann (2003), Predicting interplanetary magnetic field (IMF) propagation delay times using the minimum variance technique, *J. Geophys. Res.*, **108**, 1026, doi:10.1029/2002JA009405.

·Weygand, J.M., O. Amm, A. Viljanen, V. Angelopoulos, D. Murr, M.J. Engebretson, H. Gleisner, and I. Mann (2011), Application and Validation of the Spherical Elementary Currents

Systems Technique for Deriving Ionospheric Equivalent Currents with the North American and Greenland Ground Magnetometer Arrays, *J. Geophys. Res*., **116**, doi:10.1029/2010JA016177.

·Xing, X., J. Liang, E. Spanswick, L. Lyons, *and* V. Angelopoulos *(*2013*)*, Auroral wave structures and ballooning instabilities in the plasma sheet, *J. Geophys. Res. Space Physics*, **118**, 6319–6326, *doi:*10.1002/2013JA019068.

·Yamamoto, T., K. Makita, M. Ozaki, C.-I. Meng (1993), A particle simulation of auroral omega bands and torch-like structures, *J. Geomagn. Geoelectr*., 45, 619.

·Zesta, E., L. R. Lyons, and E. Donovan (2000), The auroral signature of Earthward flow burst observed in the Magnetotail, *Geophys. Res. Lett.*, **27**, 3241.

Tables

Table 1. Summary of the 5 intervals of omega bands observed in the THEMIS ASIs. The time period for the omega bands is given in the middle column and the imagers that clearly show omega bands are given in the third column.

Omega Band Interval	Time Period	All Sky Imagers
1	0439 UT to 0443 UT	KAPU
2	0502 UT to 0511 UT	GBAY
3	0611 UT to 0631 UT	TPAS, GILL, PINA, KAPU
4	0645 UT to 0658 UT	GILL, PINA, KAPU, SNKQ
5	0825 UT to 1054 UT	ATHA, TPAS, GILL

Table 2. Summary of the results of the power spectral analysis of the pulsations observed in the eastward component of the GOES magnetic field. The time period given in the second column is the interval used to obtain the frequency/period of the pulsations. The spacecraft are ordered from dusk to dawn.

Spacecraft	Time Period	Frequency	Period
GOES 11	0932 – 0948 UT	16.7 mHz	59.9 s
GOES 13	0944 – 0950 UT 1010 – 1050 UT	13.9 mHz 5.6 mHz	71.9 s 178.6 s
GOES 12	0900 – 1000 UT 1010 – 1050 UT	5.6 mHz 5.6 mHz	178.6 s 178.6 s
GOES 10	0900 – 1000 UT 1010 – 1050 UT	5.6 mHz 5.6 mHz	178.6 s 178.6 s

Figures

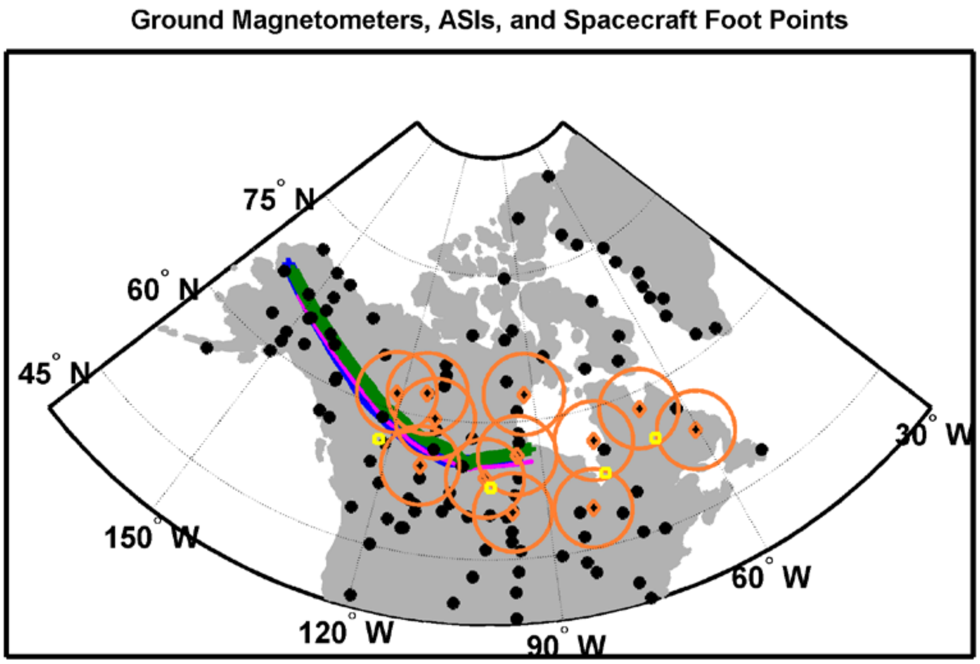

Figure 1 Distribution of ground magnetometers, all sky imagers, and spacecraft foot points across North America. The coordinate system shown is in geographic coordinates. The black dots indicate the locations of ground magnetometers with good data for the March 9th, 2008 omega bands events. The orange diamonds shows the positions of the all sky imagers used to investigate the omega bands and orange circles indicate the fields of view. The yellow squares give the average foot point locations of the GOES spacecraft determined from magnetic field line tracing for T89, T96, and T01 over the time range of 0400 UT to 1100 UT. The green, mauve, and blue curves display the THEMIS C, D, and E foot points, respectively, determined from the T01 magnetic field model from 0400 UT to 1100 UT.

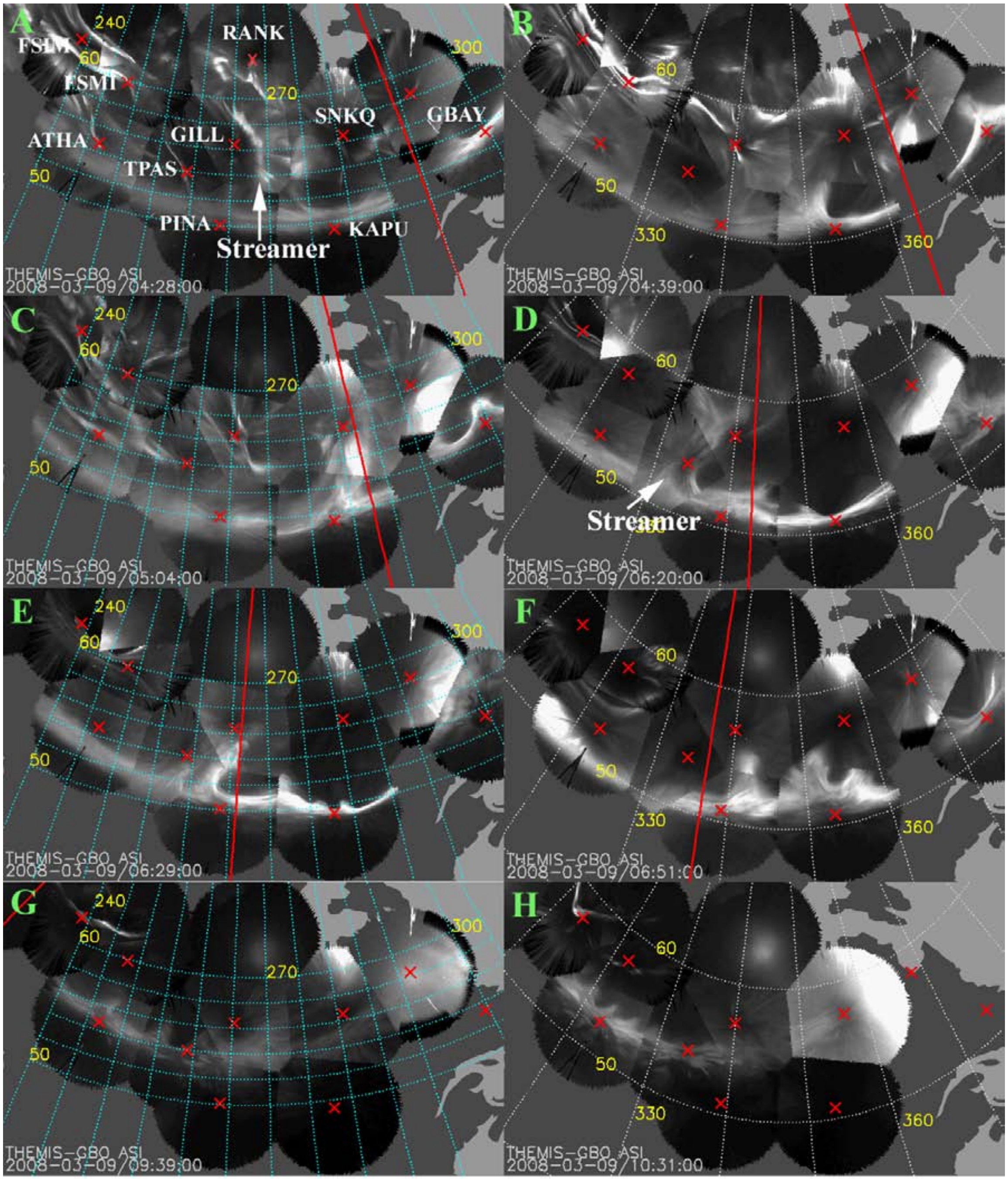

Figure 2. All sky image mosaics of streamers and omega bands observed on March 9th, 2008. The date and time of each mosaic is given in the lower left corner, the labels give geographic coordinates, and the red lines indicate local midnight. Streamers as defined in *Nishimura et al.* [2011] are present in panels A and D.

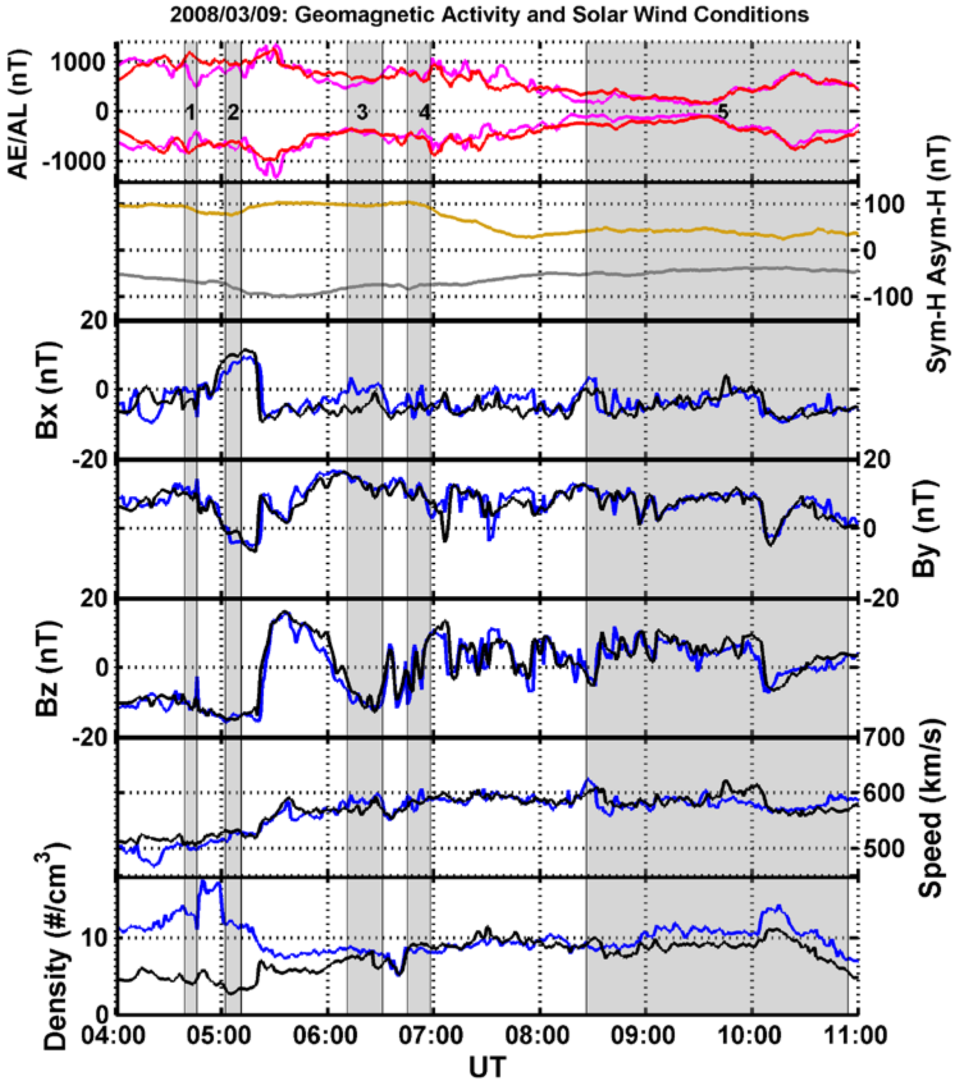

Figure 2. Geomagnetic activity and solar wind conditions during which omega band events were observed on March 9th, 2008. The top panel shows the AE and AL indices from both the standard AE index (mauve) and the THEMIS calculated AE index (red). The gray patches surrounding the numbers in the top panel indicate periods when omega bands are observed in the all sky imagers. The intervals during which the largest omega bands were observed are colored green. The second panel displays the Sym-H (gray) and Asym-H (gold) indices. The IMF *Bx*, *By*, and *Bz* are given in the third, fourth, and fifth panels where the blue curve is IMF measured at Wind and the black curve is IMF recorded at Geotail. The solar wind speed and density from Wind and Geotail are given in the final two panels.

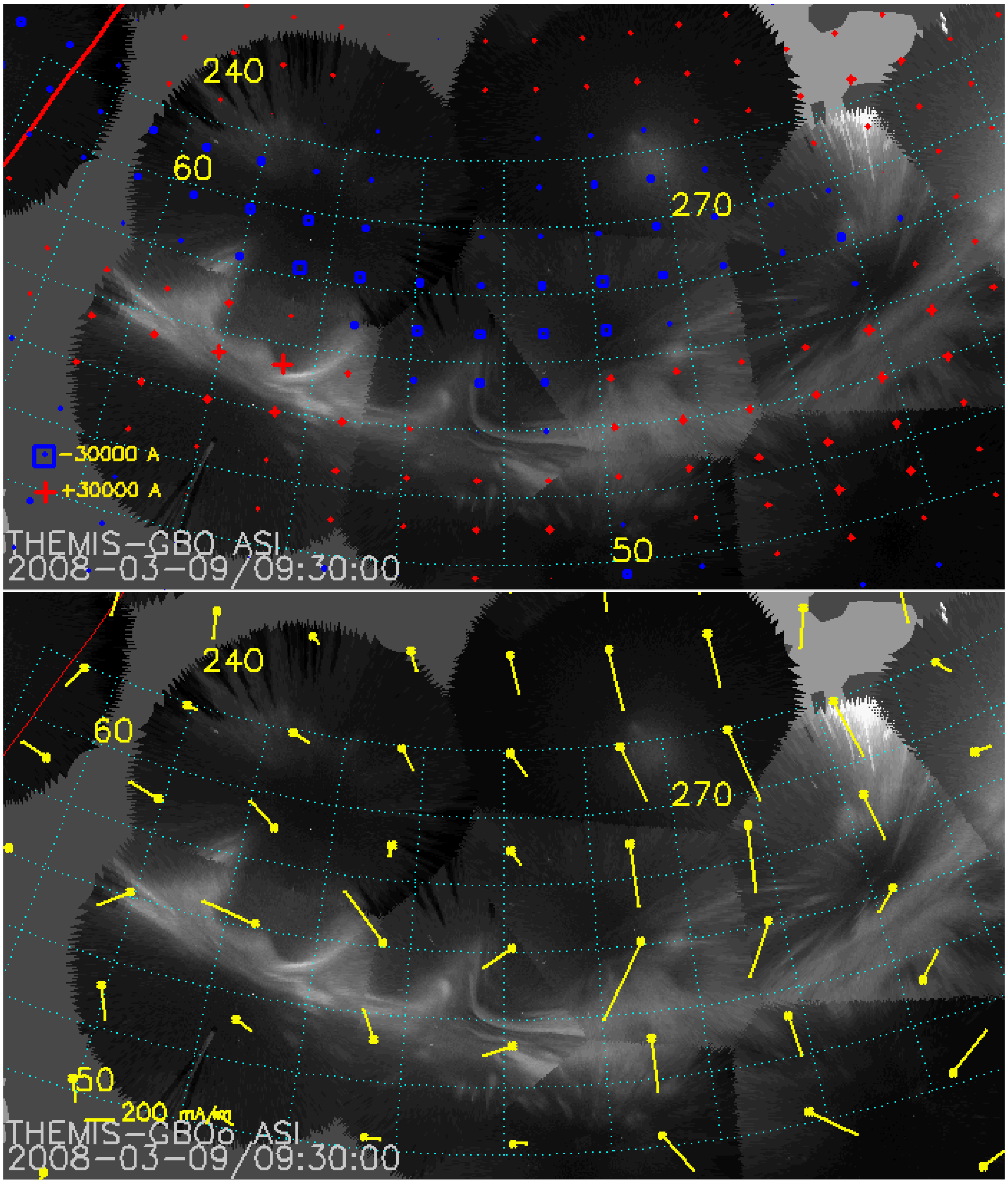

Figure 4. All sky image mosaic of omega bands observed at 0930 UT on March 9, 2008. Four omega bands are present in the ATHA (54.7° geographic north, 246.7° geographic east) and TPAS (54.0° geographic north, 259.1° geographic east) ASIs. In the top panel SEC amplitudes are shown as red plus signs and blue squares indicating upward and downward currents, respectively. The size of the symbol changes with the magnitude of the current. The key is given in the lower left corner. The equivalent ionospheric current vectors are given in yellow in the lower panel. The yellow dot shows the location at which the currents are derived. The length of the vectors changes with the magnitude of the current. The key is given in the lower left corner.

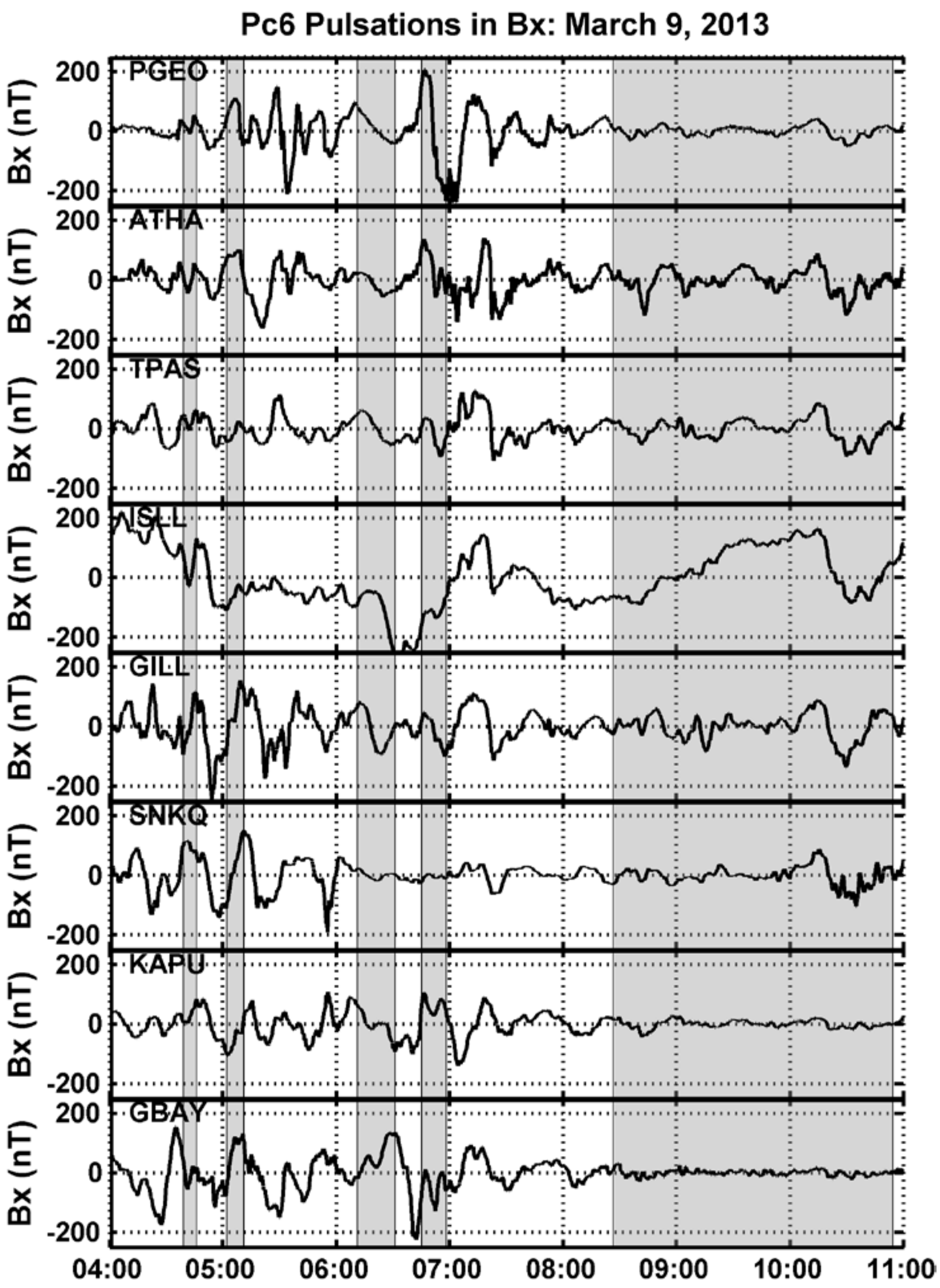

Figure 5. ***Bx*** **component from the ground magnetometers in the auroral zone near the omega bands event of March 9th, 2008. The station code is given in the upper left corner. No clear Ps6 pulsations are visible in the data.**

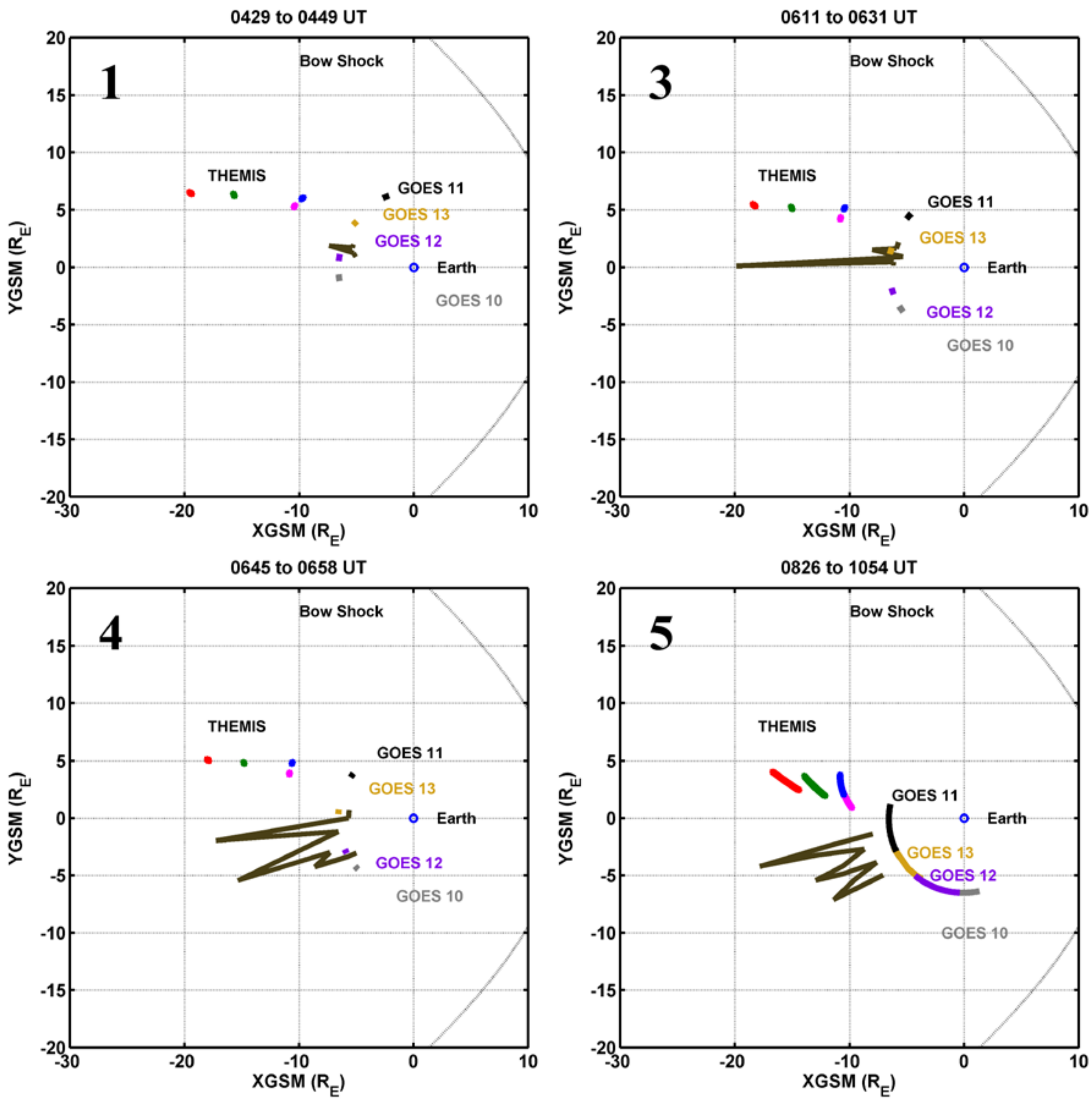

Figure 6. Spacecraft positions during the March 9th, 2008 omega band events. At about 23 MLT, THB (red) is the farthest out, THE (blue) is closest to the dusk, THD (mauve) is closest to the dawn, and THC (dark green) is between the other spacecraft. At geostationary orbit, from dusk to dawn are GOES 11 (black), GOES 13 (gold), GOES 12 (violet), and GOES 10 (gray). The black dotted line is the nominal position of the bow shock. The brown zigzag curve at about -8 Re downtail is a trace along field lines calculated from the T96 model of the poleward edges of several large omega bands from the first, third, fourth, and fifth omega band intervals.

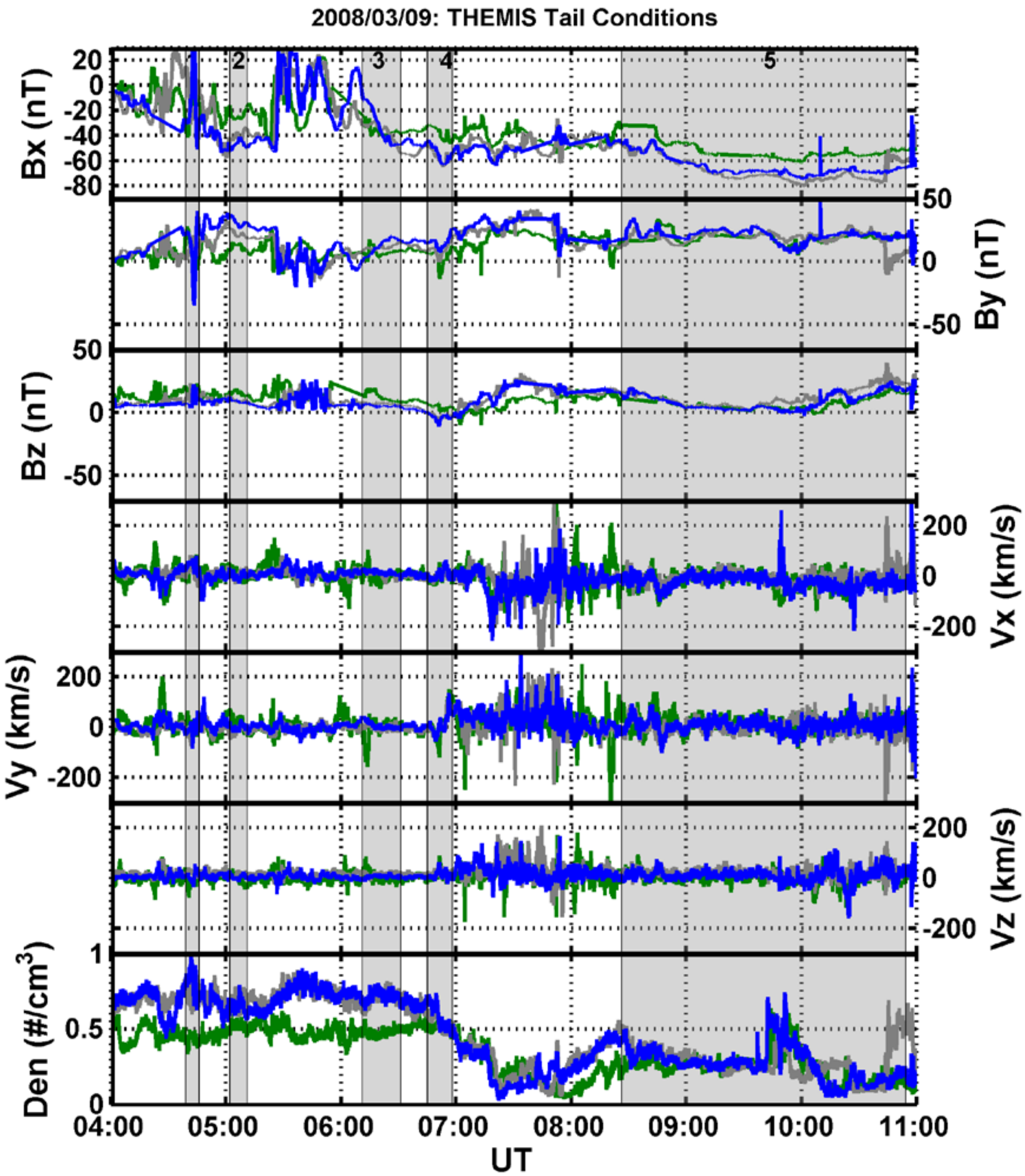

Figure 7. THEMIS magnetic field and plasma data for March 9th, 2008. The top panel shows the *Bx* GSM data from THC (green), THD (gray), and THE (blue). The second and third panels display the *By* and *Bz* components from the same spacecraft. The fourth, fifth, and sixth panels give the *Vx*, *Vy*, and *Vz* GSM components, respectively. The plasma number density is shown in the bottom panel. The gray patches surrounding numbers in the top panel indicate periods when omega bands are observed in the ASIs.

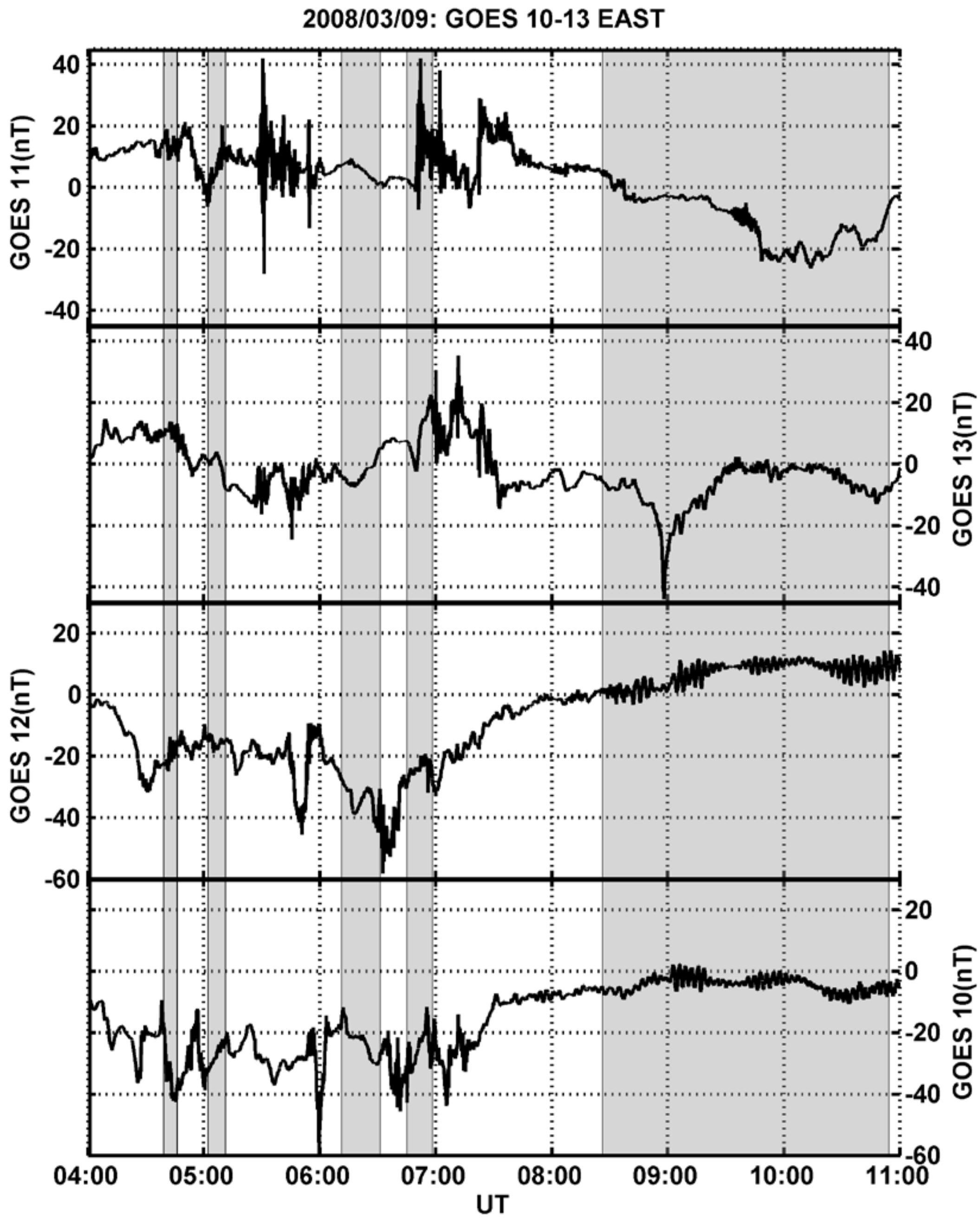

Figure 8. GOES 10-13 eastward components of the magnetic field data for March 9, 2008. These data are ordered from the most duskward spacecraft to the most dawnward spacecraft. The gray patches surrounding numbers in the top panel indicate periods when omega bands are observed in the ASIs.

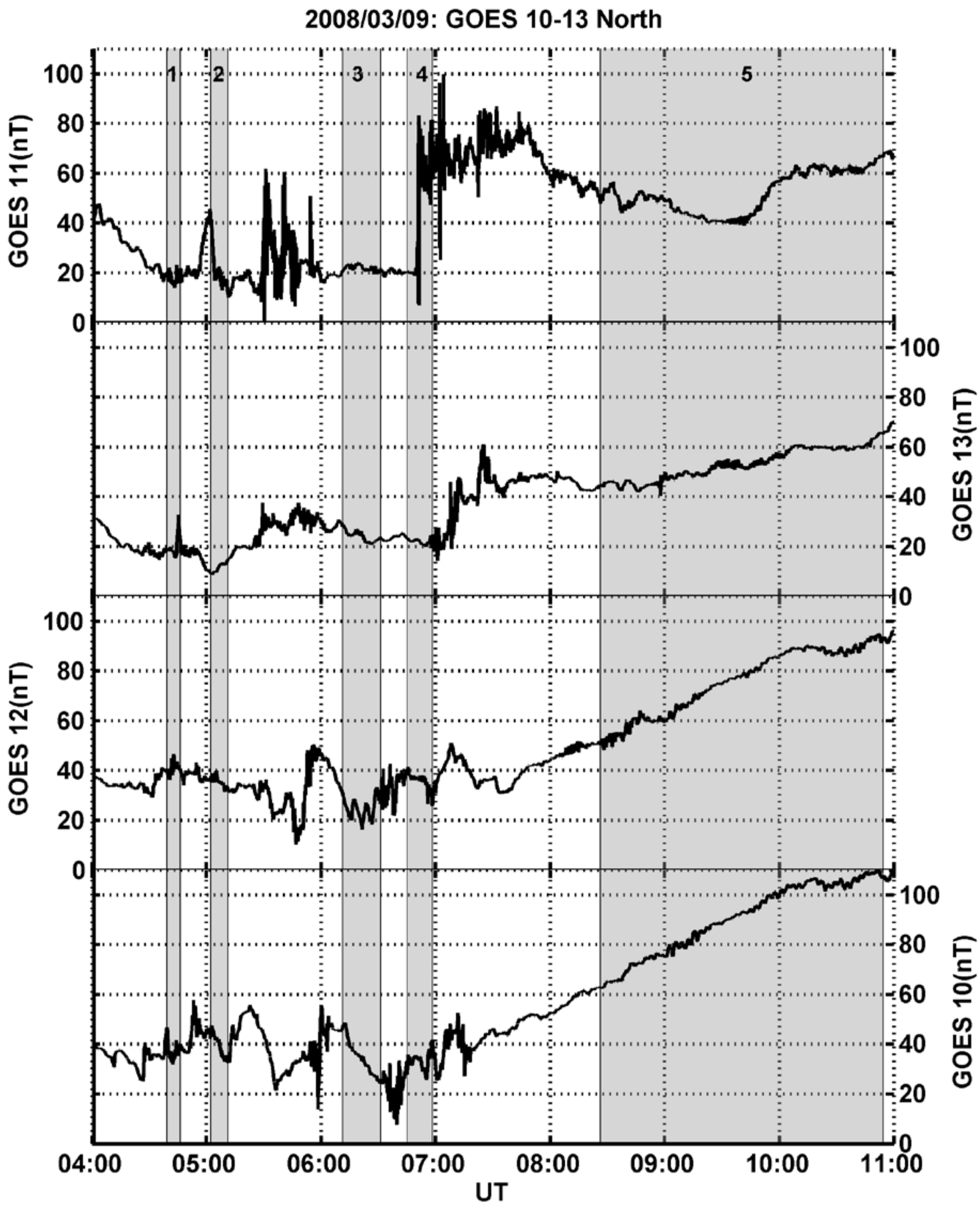

Figure 9. GOES 10-13 northward components of the magnetic field data for March 9th, 2008. This figure has the same format as Figure 7.

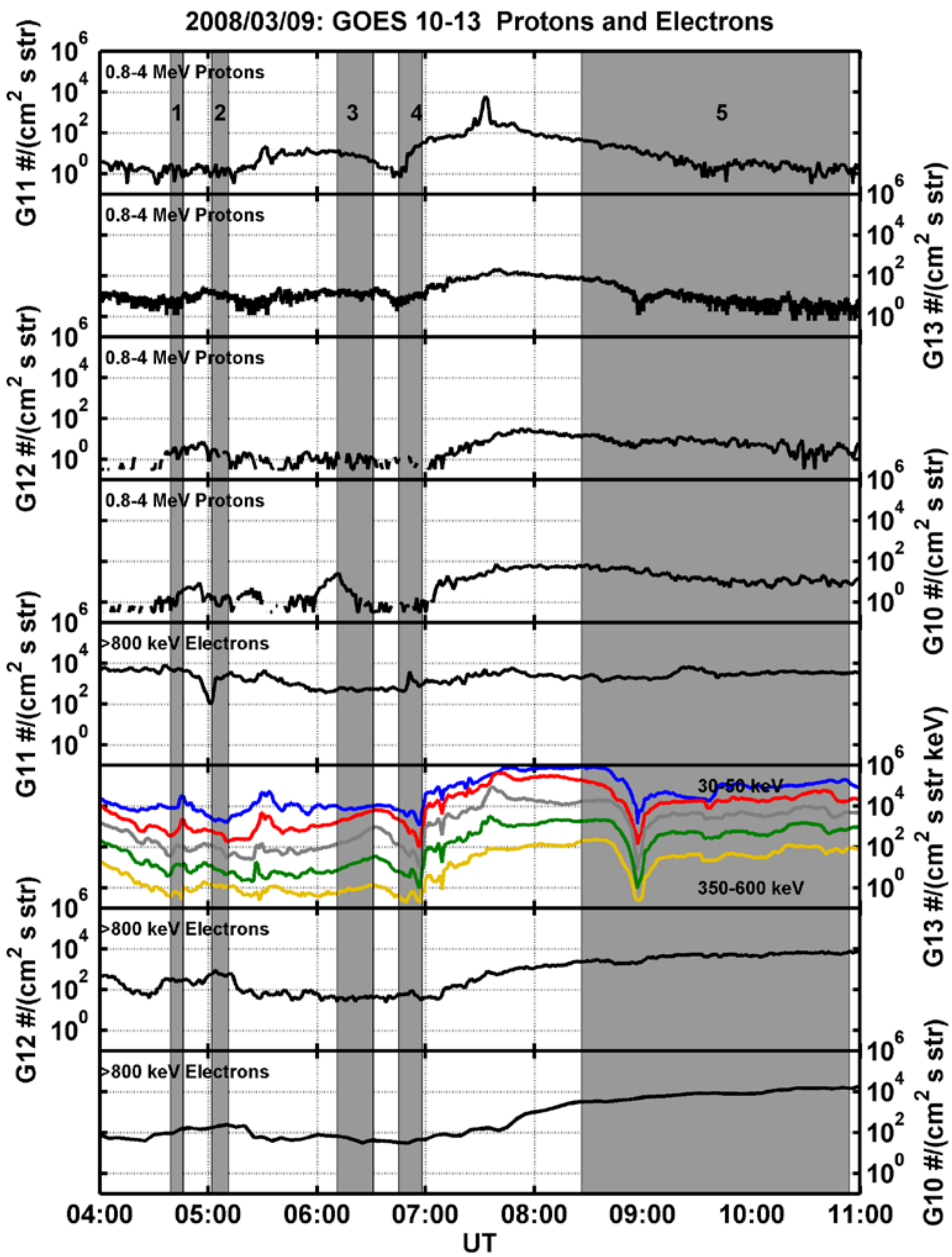

Figure 10. GOES 10-13 proton (top four panels) and electron (bottom four panels) data from March 9th, 2008. These data are ordered from the most duskward spacecraft to the most dawnward spacecraft. The spacecraft number is given on the y-axis. The particle energy range is given in the upper left corner of each panel. The gray patches with numbers indicate periods when omega bands are observed in the ASIs. Multiple curves are plotted in the 6th panel for the GOES 13 electrons for the different energy channels. Only the first and last energy channels have been labeled.

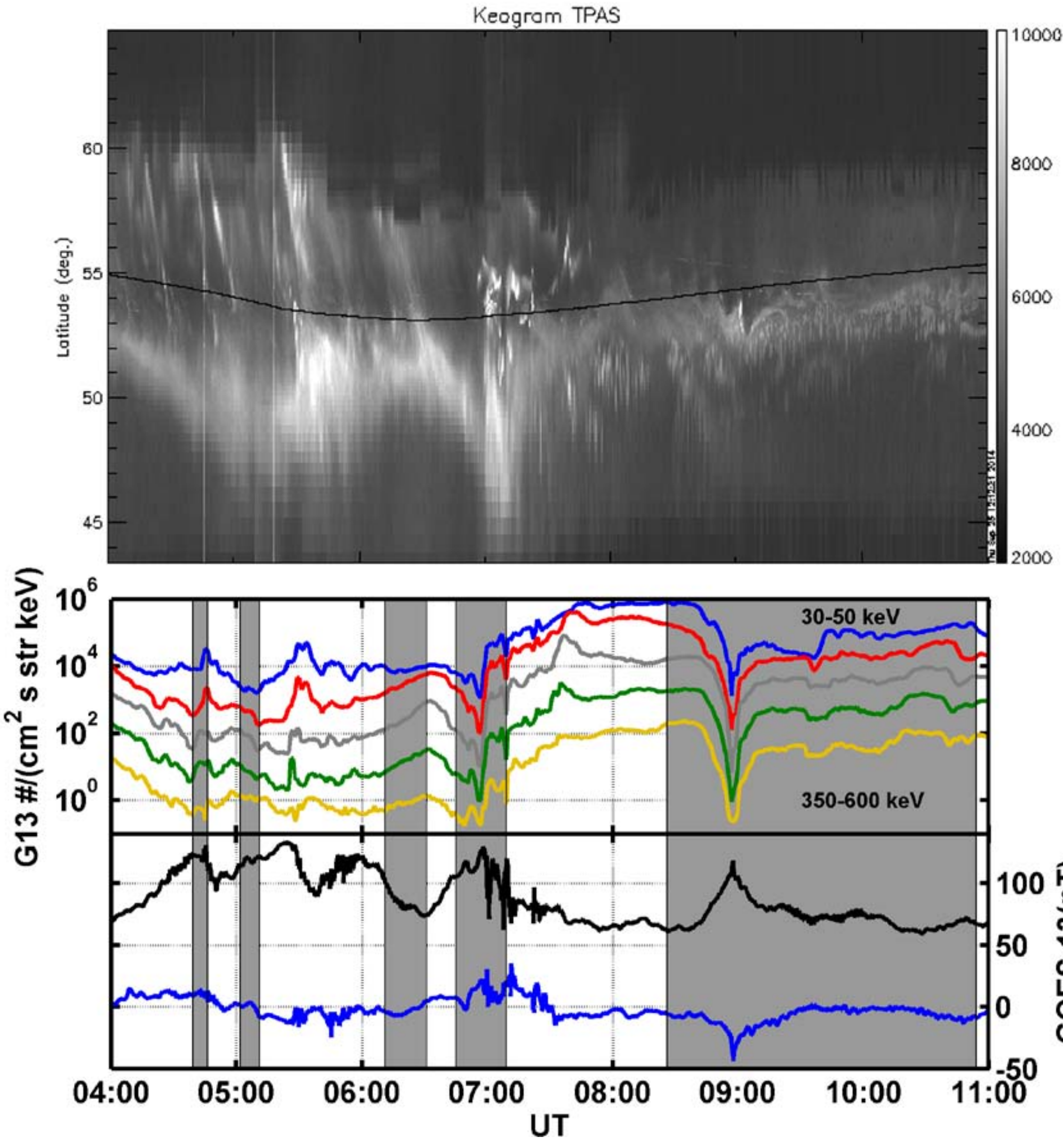

Figure 11. TPAS keogram (top panel), GOES 13 electron (middle panel) data, and GOES 13 earthward (black) and eastward (blue) magnetic field components from March 9th, 2008. The black curve in the keogram is the geographic latitude of the foot point of the GOES 13 spacecraft determined with the T01 magnetic field model. The gray patches with numbers indicate periods when omega bands are observed in the ASIs.

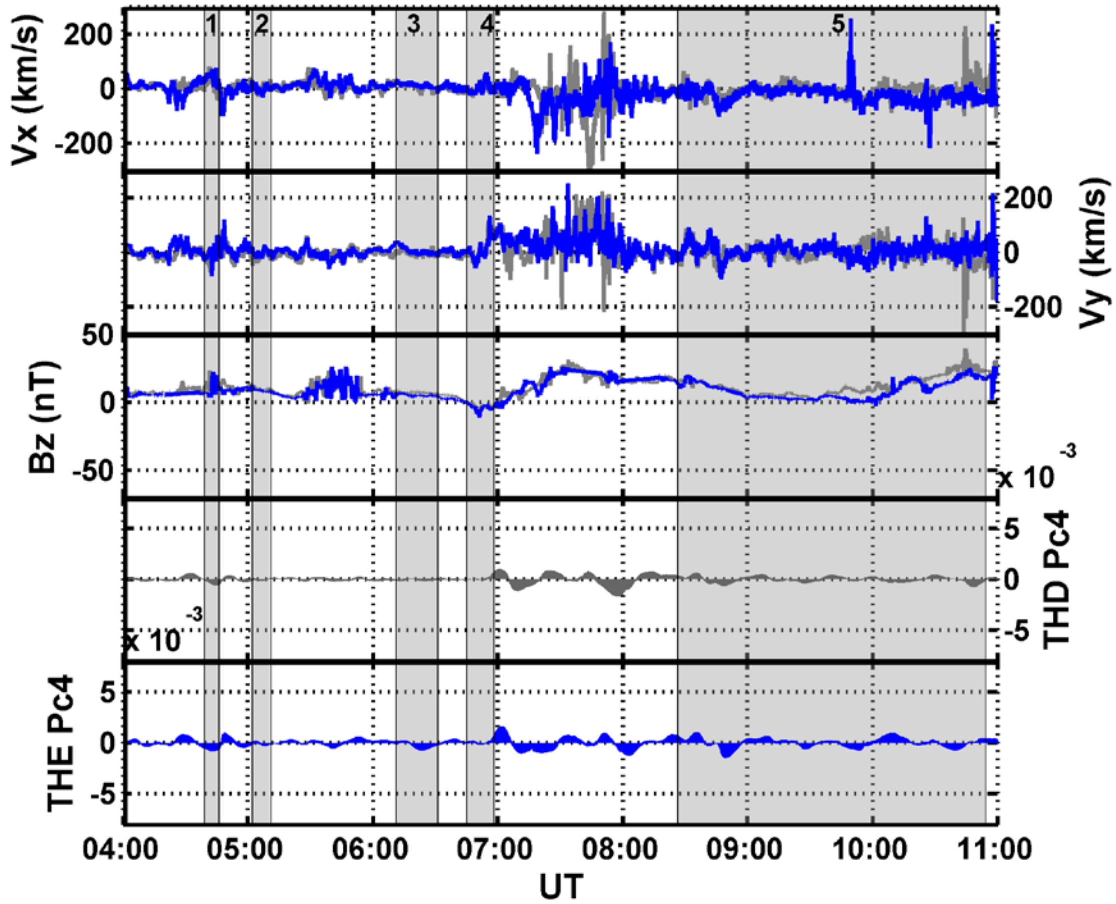

Figure 12. THEMIS magnetic field and flow data. The top two panels show the *Vx* and Vy components from THD (gray) and THE (blue) and the third panel displays the *Bz* component from the same three spacecraft. The bottom two panels are quiver plots of the *Vx* (across the time axis) and *Vy* (along the time axis) components from THD and THE that have been filtered with a Pc4 pass band filter. The gray patches delineate the 5 different omega band periods.

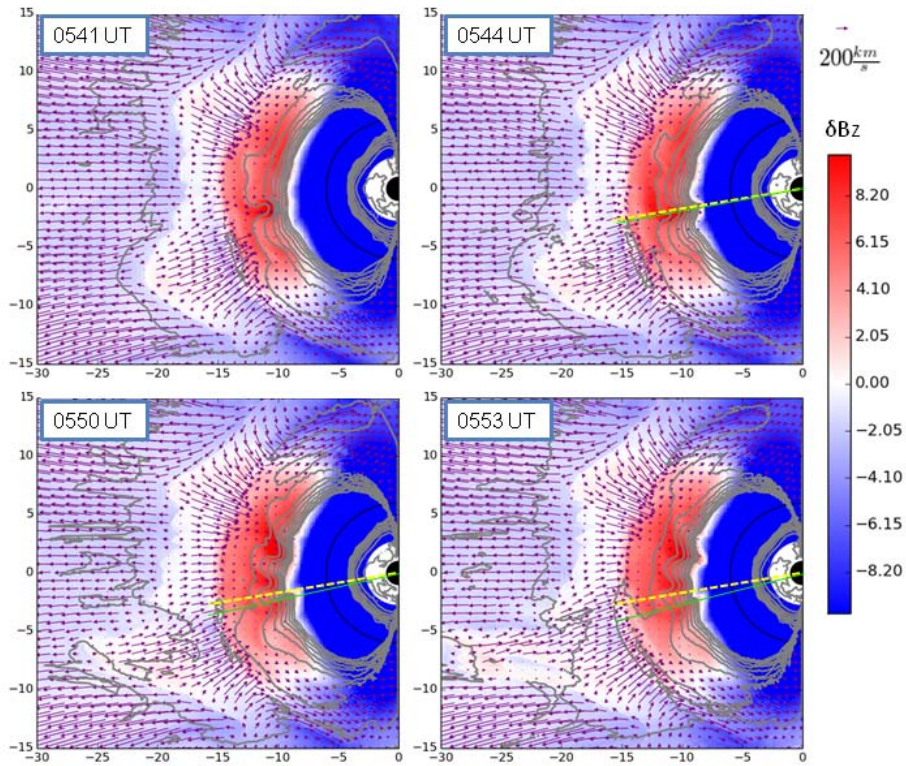

Figure 13. Results from a global MHD simulation of a substorm event that occurred on August 25, 2013. Each panel shows the flow as the purple vectors, pressure contours (gray curves), and the δBz (color) with the color bar on the right side of the figure. The yellow dashed line marks the location of a divot that has formed in the upper left panel at (-11, -2) Re. The panels appear to show high speed flows coming into the inner magnetosphere producing ripples on the inner magnetosphere that propagate to the dawnside of the magnetosphere.

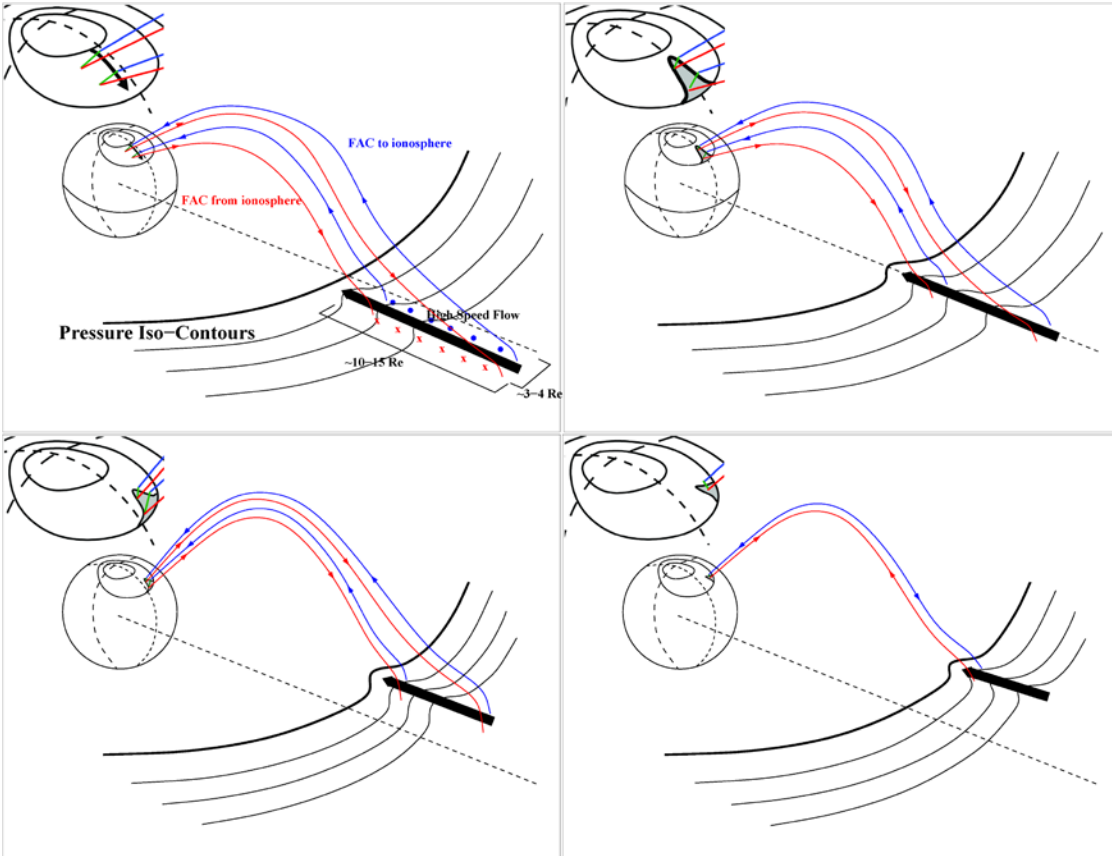

Figure 14. Interpretation of the formation of an omega band. In all four panels a high speed earthward flow is present in the tail and this flow distorts the pressure iso-contours. On the dawnside of the flow is an upward current (blue curves) from the plasma sheet to the ionosphere. An expanded view of the ionosphere and auroral oval is given in the upper left of each panel. On the duskside of the high speed flow is a current from the ionosphere to the plasma sheet (red curve). Pedersen currents connect the two field aligned currents in the ionosphere. In all four panels the omega band forms from a north south streamer into a stretched omega band that drifts eastward and gradually decreases in amplitude.